

AD-A142 067

WATER-TUNNEL STUDY OF TRANSITION FLOW AROUND CIRCULAR  
CYLINDERS(U) NATIONAL AERONAUTICS AND SPACE  
ADMINISTRATION MOFFETT FIELD C., D ALMOSNINO ET AL.

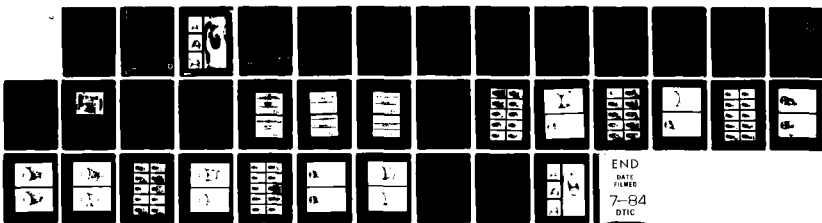
UNCLASSIFIED

MAY 84 NASA-A-9606 NASA-TM-85879

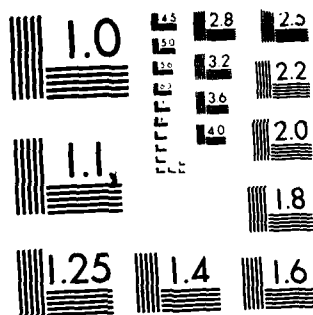
F/G 20/4

1/1

NL



END  
DATE FILMED  
7-84  
DTIC



MICROCOPY RESOLUTION TEST CHART  
NATIONAL BUREAU OF STANDARDS 1963 A

NASA  
Technical Memorandum 85879

1  
AVSCOM  
Technical Memorandum 84-A1

AD-A142 067

# Water-Tunnel Study of Transition Flow Around Circular Cylinders

D. Almosnino and K. W. McAlister

MAY 1984

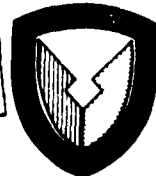
DTIC

JUN 14 1984

DTIC FILE COPY

NASA

This document has been approved  
for public release and sale; its  
distribution is unlimited.



84 06 11 060

## WAKE FROM A CIRCULAR CYLINDER



SUBCRITICAL

Almosnino & McAlister  
Ames Research Center  
Moffett Field, California

NASA

Technical Memorandum 85879

AVSCOM

Technical Memorandum 84-A-1

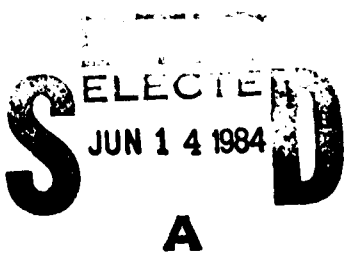
## Water-Tunnel Study of Transition Flow Around Circular Cylinders

D. Almosnino

*Ames Research Center  
Moffett Field, California*

K. W. McAlister

*Aeromechanics Laboratory  
USAAVSCOM Research and Technology Laboratories  
Ames Research Center  
Moffett Field, California*



**NASA**

National Aeronautics  
and Space Administration

Scientific and Technical  
Information Branch

1984

This document has been approved  
for public release and sale. Its  
distribution is unlimited.

## SYMBOLS

$D$	diameter of cylinder, meters	$Re$	Reynolds number, $U_\infty D/\nu$
$C_d$	drag coefficient	$St$	Strouhal number, $nD/U_\infty$
$C_l$	lift coefficient	$U_\infty$	free-stream velocity, m/sec
$n$	frequency of oscillation, Hz	$\nu$	kinematic viscosity, $\text{m}^2/\text{sec}$

Accession For	
NTIS GRA&I	
DTIC TAB	
Unannounced	
Justification	
By	
Distribution/	
Availability Codes	
Avail and/or	
Dist	Special
A1	

## WATER-TUNNEL STUDY OF TRANSITION FLOW AROUND CIRCULAR CYLINDERS

D. Almosnino\* and K. W. McAlister†

Ames Research Center and Aeromechanics Laboratory, U.S. Army Research and Technology Laboratories – AVSCOM

### SUMMARY

*The recently reported phenomenon of asymmetric flow separation from a circular cylinder in the critical Reynolds number regime has been confirmed in a water-tunnel experiment. For the first time, an attempt was made to visualize the wake of the cylinder during the transition from subcritical to critical flow and to correlate the visualizations with lift and drag measurements. The occurrence of a dominant asymmetric-flow state was quite repeatable, both when increasing and decreasing the Reynolds number, resulting in a mean lift coefficient of  $C_L \approx 1.2$  and a shift in the angle of the wake by about  $12^\circ$ . A distinctive step change in the drag and shedding frequency was also found to occur. A hysteresis was confirmed to exist in this region as the Reynolds number was cycled over the transition range. Both boundaries of the asymmetry appear to be supercritical bifurcations in the flow. The asymmetry was normally steady in the mean; however, there were instances when the direction of the asymmetry reversed and remained so for the duration of the Reynolds-number sweep through this transition region. A second asymmetry was observed at a higher Reynolds number; however, the mean lift coefficient was much lower, and the direction of the asymmetry was not observed to reverse. Introducing a small local disturbance into the boundary layer was found to prevent the critical asymmetry from developing along the entire span of the cylinder.*

### INTRODUCTION

The flow around circular cylinders has attracted the interests of scientists and engineers for many decades, not only because of its fundamental nature, but because of the succession of complex and varied wake structures that occur as the Reynolds number is varied. An extensive survey of the literature dealing with flows around circular cylinders was made by Morkovin (ref. 1), covering experimental and analytical investigations through 1964. More recently, numerous additional studies have appeared showing that a continuing variety of unanswered questions remains, and that new attempts to better understand and document the behavior of the flow are in order. For example, Achenbach (ref. 2), Jones et al. (ref. 3), and James et al. (ref. 4) have performed experiments that focused on the measurement of surface pressure, vortex shedding frequency, and the resulting aerodynamic loads; Zdravkovich (ref. 5), Perry et al. (ref. 6), and Imaichi and Ohmi (ref. 7) concentrated on flow visualization. On the other hand, rather than emphasizing measurements in specific flow regimes, Coutanceau and Bouard (ref. 8) considered the topology of flow phenomena arising during an impulsive start. Alternatively, Kiya et al. (ref. 9), Gerich and Eckelmann (ref. 10), Nakamura and Tomonari (ref. 11), and West and Apelt (ref. 12) examined, respectively, the influence of free-stream turbulence, end

plates, surface roughness and cylinder aspect ratio, and tunnel blockage. Although equally numerous and interesting, analytical and numerical attempts to calculate the flow fields around circular cylinders will not be discussed here. As so aptly stated in reference 1, the flow around a circular cylinder offers "a kaleidoscope of challenging fluid phenomena"; therefore, this introduction is intended to acknowledge only a few representative studies from among the many references on this subject.

Although the nature and origin of wake structures behind cylinders have not always been well understood, the resulting drag force has been thought to vary smoothly with speed while the lift force, albeit oscillatory, has been thought to be zero on the average. An intriguing exception to this behavior has recently been found to exist over the critical Reynolds number range for the cylinder, which extends approximately between  $2 \times 10^5 < Re < 10^6$ . Apparently sensitive to parameters such as surface roughness and tunnel turbulence level, this regime often has been characterized as having large amounts of scatter in the measured data for the aerodynamic forces and the vortex shedding frequency. Kraemer (ref. 13) was the first to report on the existence of a stable asymmetry in the flow based on measurements of the pressure distribution around a cylinder at a critical Reynolds number of  $Re = 3.6 \times 10^5$ .

This behavior was later corroborated by Bearman (ref. 14), who attributed the asymmetry to the formation of a laminar separation bubble on only one side of the cylinder. As a result of this asymmetry in the flow, it was argued that the cylinder could indeed experience such a large, nonzero

\*NASA/NRC Research Associate from Israel.

†Aeromechanics Laboratory, U.S. Army Research and Technology Laboratories – AVSCOM.

average lift force. A decade later, these findings were again confirmed by Kamiya et al. (refs. 15 and 16), using pressure measurements over a more detailed range of Reynolds numbers. The phenomenon was further investigated by Schewe (ref. 17), who not only presented force and frequency data, but also noted that, in the process of increasing the Reynolds number from subcritical to critical values, a bifurcation type of jump occurs from one flow state to another. Schewe also observed, as did Kamiya, that a hysteresis behavior in the lift and drag forces occurs as the Reynolds number decreases from supercritical to subcritical values.

The purpose of the present study is to verify in a water tunnel the flow behavior described in references 13-17, and to obtain for the first time some visualization pictures of the structure of the flow behind the cylinder in this critical Reynolds number regime. Load data are confined to measurements of the total lift and drag forces over a wide range of Reynolds numbers. Surface pressure measurements, a subject well covered in the references cited above, were not attempted in this investigation.

## DESCRIPTION OF THE EXPERIMENT

It was a goal in this experiment to study the wake flow behind a circular cylinder up to a Reynolds number of  $Re = 500,000$ . To attain this Reynolds number, given a maximum clear-tunnel speed of about 6.7 m/sec, an estimated 7.3-cm-diam cylinder would be required. However, because of the suspected operational limits of the facility in attempting to obtain this rate of flow over such a bluff body, two cylinders were constructed. One cylinder was 6.4 cm (2.5 in.) in diameter and was expected to require a flow velocity approaching the cavitation limits of the tunnel; the second cylinder was 7.6 cm (3.0 in.) in diameter and was expected to create a blockage (25%) just short of the power limits of the drive system for the speed required. Both cylinders were 21.1 cm long and spanned the test section width to within 4 mm of either side.

The models were cast of an electrically nonconducting fiber resin surrounding a stainless-steel spar. When installed, the spar extended through the test-section walls and was supported by a pair of lift- and drag-load cells on each side (fig. 1). A narrow platinum electrode, about 0.25 mm wide, was embedded in the surface of each cylinder and arranged circumferentially at the center-span location. The electrodes were segmented (fig. 2) so that individual sections could be activated independently, thereby generating hydrogen bubbles for the visualization of selected portions of the flow field. Another electrode, this one made of stainless steel, was placed upstream of the cylinder, and was oriented normal to both the axis of the cylinder and to the oncoming flow so that the predominately inviscid portion of the flow field could be visualized. The surface of the 6.4-cm-diam cylinder

was coated with a thin layer of lacquer so that the originally smooth finish on the surface would be less susceptible to erosion during the test. The 7.6-cm-diam cylinder did not receive a lacquer coating; instead it was waxed before it was installed.

This experiment was conducted in the 4,000-liter, closed-circuit, water-tunnel facility at the Aeromechanics Laboratory, Ames Research Center (fig. 3). The test section is 21 cm wide, 31 cm high, and extends horizontally a distance of 86 cm. The tunnel was pressurized to about 15 psig in order to postpone the development of cavitation bubbles that occur at the high tunnel speeds. The velocity of the water through the test section was deduced from the dynamic pressure that was obtained (approximately) from the difference between the static pressure in the settling chamber and the static pressure in the test section.

The bubbles were illuminated during photographic sessions with two broad sheets of light (about 8 mm wide), directed through the upper and lower test-section windows, and covering a distance of 30 cm in the free-stream direction. Both continuous and flash sources of light were produced over this length. The continuous source of light was provided by a single 1,000-W halogen lamp and was used for general viewing of the flow. The flash sources of light were obtained from 10,000-W xenon lamps that could either be synchronized to the shutter of a high-speed camera or be operated in a single-flash mode with a view camera.

All load-cell measurements were digitized, averaged, and displayed in coefficient form using a minicomputer. In addition, the analog signals were channeled through a 0-20,000-Hz spectrum analyzer to determine the frequency content of the data. The lift and drag loads are considered to be accurate to within 0.01 N. The calculated Reynolds number is estimated to be accurate to within 2,000. The natural resonant frequency for the model-balance combination was found to be 130 Hz (accurate to within 2 Hz). This frequency was judged to be an order-of-magnitude higher than the anticipated Strouhal frequencies for the cylinder over the Reynolds number range planned for this experiment.

## DISCUSSION OF RESULTS

### Average Loads

Most of the digitized load measurements were taken over a data-sampling interval of 60 sec, and at a rate of 360 data points per second. These data records were taken while both ascending and descending through the critical Reynolds number range, in order to identify the extent of the hysteresis effect that had been reported to exist in the flow. A typical behavior, in terms of the average lift and drag coefficients, over the range of Reynolds numbers considered in this

investigation is shown in figure 4 for the 6.4-cm-diam cylinder. The average lift coefficient remains zero as long as the cylinder is in the subcritical flow regime, shedding vortices periodically up to  $Re \approx 250,000$ . At this point, the flow around the cylinder undergoes a change that causes the shedding frequency and amplitude to be markedly altered (beginning of critical regime). Then, at  $Re = 290,000$ , the flow begins to develop a small asymmetry, as evidenced by a modest growth in the average lift coefficient. An examination of other characteristics of the lift curve, to be presented below, will suggest that this behavior is consistent with a supercritical bifurcation. The drag coefficient, which has already been decreasing with increasing Reynolds number, shows no obvious departure from this trend. However, as the Reynolds number is increased to  $Re = 310,000$ , the slopes of the lift and drag curves begin to change more rapidly. When the Reynolds number is increased further, but only by a small amount, there is an abrupt jump in the average lift coefficient to a value of  $C_L \approx 1.2$  at  $Re = 315,000$ . Simultaneously, the average drag coefficient abruptly decreases to a value of  $C_d = 0.8$ . This jump is typical of a classical bifurcation that occurs between two equilibrium flow states (ref. 18). At this stage the flow is asymmetric in the mean (critical asymmetric), its direction being initially determined at random. The flow normally remains aligned in this direction, unless a sufficiently large disturbance in the flow is encountered. Since the separation from the cylinder could have been in either direction, the condition of asymmetry is considered to be bistable.

In the case of the 6.4-cm-diam cylinder, this region of asymmetry continues up to  $Re \approx 345,000$  (fig. 4). At this point, the average lift coefficient returns to near zero and the average drag coefficient rapidly decreases to a minimal value ( $C_d \approx 0.44$ ). The flow is again symmetric in the mean (supercritical symmetric). At  $Re \approx 400,000$  there is a second, although much smaller, rise of the average lift coefficient to a value of  $C_L \approx 0.3$  (with some scatter in the repeatability), along with a small rise in the average drag coefficient (supercritical asymmetric). This phenomenon was also reported in references 15 and 16, but not in reference 17. In the present experiment, it was not possible to increase the Reynolds number beyond  $Re = 520,000$  for this cylinder. However, the data from references 15 and 16 indicate that this second asymmetry decays gradually up to  $Re = 700,000$ , where the average lift coefficient becomes zero again. Some possible explanations for this asymmetry will be discussed later.

When decreasing the Reynolds number through the asymmetric region and into subcritical flow, it is clear from figure 5 that a hysteresis exists in the curves for the average lift and drag coefficients. The fact that both faces of the asymmetry are shifted indicates that two bifurcations are present: one at the subcritical-critical interface; the other at the critical-supercritical interface. At both interfaces there is a growth in the curve in the direction of the asymmetry (especially obvious in the lift coefficient) that suggests that

both bifurcations are supercritical. It should be noted that the bifurcations reported in reference 17 are of the subcritical class. Based on measurements from the present experiment, the proposed bifurcations for the lift and drag coefficients are shown in figure 6.

In some cases, the flow was observed to choose, for the asymmetry, the opposite direction from that chosen when the Reynolds number was increasing (see also refs. 15-17). As discussed earlier, an occasional disturbance in the flow was apparently large enough to cause the flow to switch sides in the asymmetric flow regime (fig. 7). However, the positive and negative  $C_L$  peaks were essentially equal in magnitude and Reynolds number of occurrence. This kind of behavior has not been previously documented in the literature. The authors believe that this phenomenon can be attributed either to inadvertent flow disturbances in the free stream (which are both intermittent and large scale) or to an ever-changing condition in the quality of the surface on the cylinder. It was found, for example, that a similar switch in the asymmetry could be provoked by rotating the cylinder to a different angle. This is perhaps not too surprising when considering the extreme sensitivity of separation to surface roughness in the transition zone.

### Oscillating Loads

The instantaneous loads were also examined using a frequency analyzer. An example of the typical behavior of the loads at various Reynolds numbers in the subcritical, critical, and supercritical flow regimes appears in figure 8: they were obtained using the 7.6-cm-diam cylinder. Attention should be focused more on the different flow states shown for the 7.6-cm-diam cylinder than on the actual Reynolds numbers at which they occur. Otherwise, some discrepancy might be suspected when comparing these results with those shown in figure 4 for the 6.4-cm-diam cylinder. An explanation for the difference in Reynolds numbers between the two cylinders in each of the flow regimes will be presented in a later section. Furthermore, the traces appearing in figures 8(a)-8(f) are not to be compared with each other on an absolute basis. Although the amplifications are the same throughout this set of figures, the reference levels were shifted as required (especially during the asymmetric range) to keep the traces within the limits of the display. It is interesting to note the change in the pattern of the lift trace when passing from the subcritical regime, where oscillations appear to have a fairly definite periodicity, to the critical regime, where the amplitude of the oscillations becomes much smaller and the frequency appears more random (similar to the critical-fluctuation results of ref. 17). Another interesting phenomenon is the long-wave "beat" which gives an undulating appearance to the envelope of the lift force oscillations (fig. 8(b)). This phenomenon has been reported to exist on finite-span cylinders in tunnel experiments (ref. 10). When

the frequency analyzer was applied to the lift data (using the 6.4-cm-diam cylinder), very definite frequencies could be detected throughout the subcritical flow regime (fig. 9). The corresponding Strouhal number was  $St = 0.20$  at the lower Reynolds numbers; it increased gradually to  $St \approx 0.26$  toward the end of the subcritical region.

Beyond the subcritical flow regime, and especially when the flow was asymmetric, the frequency analysis did not yield a very distinctive shedding frequency above the level of broadband noise. It should be noted that this result is not in agreement with the analyses reported in references 14 and 17, in which more distinct peaks were observed. One possible reason for this difference is the presence of higher (although not quantified) free-stream turbulence levels in the present study, compared with the very low turbulence levels reported in references 14 and 17. Another possible explanation is that the high broadband noise level in the present experiment could have obscured the presence of any small amplitude oscillations. A high level of noise, as explained in reference 14, could also produce a sufficient amount of scatter in the data to prevent the detection of weak oscillations. A final point of disagreement with references 14 and 17 concerns the level of the Strouhal number and the shift in its variation with Reynolds number (fig. 9). These differences are believed to be due to differing blockage effects in the tunnels.

### Flow Visualization

One of the main objectives in the present study was to gain some understanding of the structure of the flow around a cylinder, particularly the asymmetric flow in the critical Reynolds number regime. Although references 13-17 provide a great deal of quantitative data within this regime, it is not possible to deduce the structure of the flow from this body of data. A better understanding of the flow mechanisms causing the asymmetry is clearly needed. Moreover, the importance of this understanding may be even greater when considering the topologies of Reynolds-number-dependent events, and the analogies between transient flows around cylinders and steady flows around bodies of revolution at high incidence.

The necessity of adopting a segmented surface electrode became evident during preliminary tests in the critical regime. It was found that when an electrode that extended completely around the circumference of the cylinder was activated, it usually destroyed the asymmetry in the flow (results not shown). Furthermore, even though the width of the electrode was negligible compared with the span of the cylinder, an immediate and large change in the average lift and drag measurements occurred when the electrode was activated. Although it was necessary to modify the model before continuing the experiment, a significant lesson was provided by this experience.

Before this point is discussed, however, a short digression is in order. As explained in reference 14, the asymmetry in the flow is *believed* to be due to the formation of a single laminar-separation bubble on one side of the cylinder. This bubble is described as a region where the laminar layer detaches, undergoes transition to turbulence, and then reattaches farther around the cylinder circumference. The flow then continues as a turbulent-boundary layer and eventually separates. At the same time, on the other side of the cylinder, the flow is still laminar before separation. Since laminar and turbulent boundary layers are known to separate at different points around a cylinder, an asymmetry is formed in the flow.

With this description in mind, we will continue the discussion of the electrode effects in the present experiment. First, it appears that the hydrogen bubbles may have acted much like a boundary-layer trip, therefore supporting the notion that transition (on only one side) is responsible for the asymmetry. It is not possible, however, to draw from this statement any definite conclusions about the existence of a single laminar-separation bubble, since it is sufficient that the boundary layer merely be turbulent at separation to cause an asymmetry. In other words, the boundary layer on one side could have become turbulent because of a trip downstream of the leading-stagnation point, therefore causing an asymmetric wake. Second, it appears that transition at any point along the span causes a disruption of the flow along its entire length, thereby preventing the formation of symmetric and asymmetric separation cells along the span of the cylinder. This observation could be significant in that it would support the notion of a single laminar-separation bubble, if it can be shown that laminar-separation bubbles are less amenable to segmentation from locally forced transitions than are laminar boundary layers (which are known to readily permit turbulent zones).

By activating only those electrodes over the leeward portion of the cylinder, bubbles could be released into the wake without affecting the asymmetry. Although such a restricted release of bubbles did not seem to be necessary during the symmetric flow cases, this limited selection of electrodes nevertheless was not changed over the complete Reynolds number range in order to establish a measure of consistency. It may be significant to recall this fact when evaluating the structure of the flow in the photographs, since only the wake region (as bounded by the separation streamlines) will be visible. Visualization of boundary-layer details, most importantly those concerning the laminar separation bubble, will not be possible in this experiment. Since the current explanation for the origin of the critical asymmetry is founded on the existence of a single laminar-separation bubble, subsequent visualization experiments must be carefully designed to avoid provoking transition in the boundary layer. The use of hydrogen bubbles may still be considered as a candidate technique; however, the bubbles should be generated at a reduced rate and only at discrete locations along the

surface where the separation bubble is believed to occur. Dye injection from the surface of the cylinder is an alternative technique that should provide a good definition of the laminar portion of the boundary layer. In this case, shaping the exit port and tailoring the dye pressure are important considerations that must be addressed in order to prevent unintentional disturbances to the flow.

The electrode that was placed in the free stream ahead of the cylinder produced bubbles that did not become part of the formation of the boundary layer and remained essentially outside of the wake region near the cylinder. Although the flow visualizations that were obtained with this electrode did reveal the boundaries of the entire separated region behind the cylinder during the asymmetric range, they did not contribute much to an understanding of the wake structure. Maintaining an electrode in the stream also proved to be inconvenient owing to frequent breaks in the wire resulting from the large loads that occur at the higher tunnel speeds.

### Specific Flow Regimes

In many of the following visualization pictures, the flow will appear as a collection of segmented path-lines rather than as point images. This streaking effect was intentionally created by protracting the light from the strobe over an extended period of time (ref. 19) in order to capture the vortical content of the flow. The sequence of pictures contained in figures 10-19 was obtained with the 6.4-cm cylinder and was derived from both the view camera and from sections of movie film taken at 64 frames/sec. When examining the figures containing a sequence from a movie film, it should be noted that the presentation is contiguous (all frames in the sequence included) and that the organization is from top-to-bottom and from left-to-right.

**Subcritical symmetric**— At a typical subcritical Reynolds number of  $Re = 144,000$ , the flow is shedding a well-known von Karman vortex street, with a corresponding Strouhal number of  $St = 0.21$  (fig. 10). If the first scene in this sequence is considered to coincide with the beginning of an oscillation cycle, the last scene appears to complete one period of oscillation in the vortex-shedding process. The corresponding path-line exposures for this flow are shown in figure 11.

**Critical onset**— As the Reynolds number is increased, the frequency of the shedding also increases until reaching  $Re \approx 308,000$ . At this point, the shedding seems to become less regular (fig. 12), and the lift-force oscillations become greatly reduced (see also fig. 8(d) for behavior in corresponding flow regimes on the larger cylinder). A typical example of this flow is shown in figure 13; it is probably also representative of stages "a-b" described in reference 17. It is evident from figures 12 and 13 that vortical shedding is still

occurring. However, the time-history for the loads (fig. 8(d)) and the results from the spectrum analysis show that the shedding frequency is not very steady. One possible explanation for this shedding irregularity is that the conditions for transition to turbulence in the free-shear layer are only intermittently satisfied. Another reason for this unsteady behavior may have been the tunnel noise level, which was apparently higher in the present experiment than it was for the wind-tunnel measurements reported in references 14-17. The noise level seemed to increase as the velocity was increased, so that the last remark applies to all of the following data.

**Critical asymmetric**— When the tunnel speed was increased further, the flow abruptly changed to the asymmetric mode, and generally persisted in that state between  $Re = 315,000$  and  $Re = 350,000$  (for the 6.4-cm cylinder). The corresponding movie sequence appears in figure 14, where the asymmetry is shown to be clearly present in the mean. Although this asymmetry was found to be quite sensitive to upstream disturbances in the boundary layer (recall the influence of the bubbles from the surface electrode on the windward side of the cylinder), it is interesting to note the relative insensitivity of the separation points to the unsteadiness in the wake just downstream of the cylinder. Vortical shedding occurs in this regime as well, as can be seen from both the movie sequence (fig. 14) and the path-line pictures (figs. 15(a)-15(f)). This region is equivalent to stages "c-e" in reference 17.

The frequency measurements indicate that although the shedding process in this asymmetric region is not very regular, a Strouhal number of  $St \approx 0.37$  (for the 6.4-cm cylinder) can be detected. This number is higher than the one reported in references 14 and 17 ( $St \approx 0.33$ ) for the same flow regime, and is believed to be due to the larger blockage and wall effects in the present study. The flow in the wake of the cylinder was observed to be highly three-dimensional. This may have obscured to some extent the clarity of the vortical structures in the path-line photographs, as well as have contributed to the irregular nature of the shedding in this range. A final comment on the character of the asymmetric region concerns the direction of the asymmetry. The randomness in the direction chosen by the flow was observed many times during the experiment; an example of one such occurrence is presented in figures 15(b) and 15(c). As mentioned earlier, the direction of the asymmetry appears to be random, depending on the momentary local surface conditions and disturbances in the flow. However, once a direction was established, the flow would remain in this direction unless a sufficiently large disturbance was encountered to cause it to shift.

**Supercritical symmetric**— Increasing the Reynolds number to  $Re \approx 360,000$  presumably caused the laminar-separation side of the cylinder to develop instead a laminar-separation

bubble (and hence a transition to turbulence) before separating (ref. 14). In other words, the flow over the surface of the cylinder now has two laminar-separation bubbles, and is therefore (once again) symmetric in the mean (stage "f" in ref. 17). The wake region close to the cylinder is relatively steady, but oscillations do exist farther downstream (fig. 16). The path-line photographs (fig. 17) show the existence of a pair of large vortices, and also the existence of shear-layer fluctuations at the edges of the wake. Frequency spectra show a weak periodic shedding, corresponding to a Strouhal number of  $St \approx 0.52$  (for the 6.4-cm cylinder) in the present study (compared with  $St = 0.45$  in refs. 14 and 17).

**Supercritical asymmetric**— Even at the much higher Reynolds number of  $Re = 520,000$ , the two laminar separation bubbles are assumed to still be present. However, the separation points have moved up the shoulders of the cylinder, and the wake has become wider (fig. 18). Load measurements normally show a small asymmetry in the flow, the cause of which is not obvious (see also refs. 15 and 16). The path-line photographs (figs. 19(a)-19(d)) show this small asymmetry, particularly in the wide-angle views (figs. 19(a) and 19(b)). One possible explanation for this asymmetry is that the two bubbles are almost always in different stages of development; that is, one bubble develops at an earlier azimuthal position than the other. The phenomenon should be very sensitive to local surface conditions, and indeed there is more scatter in the average lift measurements in this regime. Although the periodic shedding is very weak, the Strouhal number for this region is  $St \approx 0.52$  (as in the lower-Reynolds-number region), and this behavior is consistent with that reported in references 14 and 17 (although for a lower Strouhal number,  $St = 0.45$ ). An examination of figure 19 indicates the existence of vortices in the wake, and apparently a growth in shear-layer fluctuations at the wake edges. It seems that these fluctuations play an important role in the shedding process within this flow regime, but the present data may be insufficient for a complete understanding of that role.

#### Turbulence and Tunnel Wall Effects

The cylinders used in the present study caused a relatively large amount of blockage in the tunnel. The blockage for the two cylinders was calculated to be 20.5% and 24.6%. This blockage effect is believed to be responsible for the shift in the critical Reynolds numbers, causing certain phenomena (like the asymmetric flow regime) to appear at lower Reynolds numbers than those reported in references 14-16 where the blockage was lower. It may also be responsible for the relative increase in the Strouhal numbers observed in the present study in the critical Reynolds number range. In spite of this effect, the load measurements indicate that the basic elements of the phenomena were not altered. It appears from

figure 20 that blockage may have a strong effect on the Reynolds number range over which the asymmetry occurs. For reference, the range of the asymmetry and the maximum level of the lift coefficient reported in references 15 and 17 are also indicated in figure 20. Note that an exact comparison cannot be made between the present results and those from references 15-17, since blockage is probably not the only controlling parameter. Other possible parameters may be the tunnel turbulence level, the cylinder-surface condition, and the rigidity of the system.

#### CONCLUSIONS

The previously reported phenomenon of asymmetric flow separation on a circular cylinder in the critical Reynolds number regime has been confirmed in a water-tunnel experiment. Although many questions remain unanswered, some additional understanding of this interesting behavior has been obtained in the present investigation.

1. For the first time, an attempt was made to visualize the wake of the cylinder flow during the transition from subcritical to critical flow, and to correlate visualizations with lift and drag measurements. That portion of the near-wake region that is bounded by the separation streamlines was observed to progressively decrease in width as each higher critical-flow state was encountered. A minimum width was attained at the supercritical-symmetric flow state, after which the width of the wake increased slightly in the supercritical-asymmetric regime.

2. The most significant event to occur during transition was in the critical-asymmetric region. The wake was observed to shift in angle about  $12^\circ$ , along with a sudden increase in the mean lift to  $C_L \approx 1.2$ . A distinctive step change in the drag and shedding frequency was also found to occur. A hysteresis was also confirmed to exist in this region as the Reynolds number was cycled over the transition range. It appears that the subcritical-critical and the critical-supercritical interfaces of the asymmetric region are supercritical bifurcations.

3. Although the critical asymmetry was normally steady in the mean, there were instances when the asymmetry switched sides and remained there for the duration of the Reynolds number sweep through the asymmetric zone. A switching of sides was not observed in the supercritical-asymmetric region.

4. Introduction of a small disturbance into the boundary layer on the windward side of the cylinder prevented the critical asymmetry from occurring. Even though this disturbance was limited to a narrow spanwise band on the cylinder, load measurements indicated that the disturbance affected the asymmetry over the entire span.

5. The boundary layer was not visualized in this experiment. Since the current explanation for the origin of the

critical asymmetry is founded on the existence of a single laminar-separation bubble, it is recommended that subsequent experiments be focused on this region. Both hydrogen bubble and dye injection are candidate visualization techniques; however, care must be taken to avoid provoking transition in the boundary layer.

Ames Research Center

National Aeronautics and Space Administration  
Moffett Field, California 94035, January 30, 1984

REFERENCES

1. Morkovin, M. V.: Flow Around Circular Cylinder - A Kaleidoscope of Challenging Fluid Phenomena. ASME Symposium on Fully Separated Flows, 1964.
2. Achenbach, E.: Distribution of Local Pressure and Skin Friction around a Circular Cylinder in Crossflow up to  $Re = 5 \times 10^6$ . J. Fluid Mech., vol. 34, 1968, pp. 625-639.
3. Jones, G. W., Jr.; Cincotta, J. J.; and Walker, R. W.: Aerodynamic Forces on a Stationary and Oscillating Circular Cylinder at High Reynolds Numbers. NASA TR R-300, 1969.
4. James, W. D.; Paris, S. W.; and Malcolm, G. N.: Study of Viscous Crossflow Effects on Circular Cylinders at High Reynolds Numbers. AIAA J., vol. 18, Sept. 1980, pp. 1066-1072.
5. Zdravkovich, M. M.: Smoke Observations of the Formation of a Karman Vortex Street. J. Fluid Mech., vol. 37, 1969, pp. 491-496.
6. Perry, A. E.; Chong, M. S.; and Lim, T. T.: The Vortex Shedding Process behind Two-Dimensional Bluff Bodies. J. Fluid Mech., vol. 116, 1982, pp. 77-90.
7. Imaichi, K.; and Ohmi, K.: Numerical Processing of Flow-Visualization Pictures - Measurement of Two-Dimensional Vortex Flow. J. Fluid Mech., vol. 129, 1983, pp. 283-311.
8. Coutanceau, M.; and Bouard, R.: Experimental Determination of the Main Features of the Viscous Flow in the Wake of a Circular Cylinder in Uniform Translation. Part 1. Steady Flow; Part 2. Unsteady Flow. J. Fluid Mech. vol. 79, 1977, pp. 231-256, 257-272.
9. Kiya, M.; Suzuki, Y.; Arie, M.; and Hagino, M.: A Contribution to the Free-Stream Turbulence Effect on the Flow Past a Circular Cylinder. J. Fluid Mech., vol. 115, 1982, pp. 151-164.
10. Gerich, D.; and Eckelmann, H.: Influence of End Plates and Free Ends on the Shedding Frequency of Circular Cylinders. J. Fluid Mech., vol. 122, 1982, pp. 109-121.
11. Nakamura, Y.; and Tomonari, Y.: The Effects of Surface Roughness on the Flow Past Circular Cylinders at High Reynolds Numbers. J. Fluid Mech., vol. 123, 1982, pp. 363-378.
12. West, G. S.; and Apelt, C. J.: The Effects of Tunnel Blockage and Aspect Ratio on the Mean Flow Past a Circular Cylinder with Reynolds Numbers between  $10^4$  and  $10^5$ . J. Fluid Mech., vol. 114, 1982, pp. 361-377.
13. Kraemer, K.: Druckverteilungsmessungen an Kreisrunden mit Beachtung dreidimensionaler Randbedingungen. Mitt. MPI f. Stromungsforschung und Aerodynamischen Versuchsanstalt, Gottingen No. 32, 1965.
14. Bearman, P. W.: On Vortex Shedding from a Circular Cylinder in the Critical Reynolds Number Regime. J. Fluid Mech., vol. 37, 1969, pp. 577-585.
15. Kamiya, N.; Suzuki, S.; and Nishi, T.: On the Aerodynamic Force Acting on a Circular Cylinder in the Critical Range of the Reynolds Number. AIAA Paper 79-1475, July 1979.
16. Kamiya, N.; Suzuki, S.; Nakamura, M.; and Yoshinaga, T.: Some Practical Aspects of the Burst of Laminar Separation Bubbles. ICAS Paper 80-10.2, Proc. of the 12th Congress of ICAS, Munich, Federal Republic of Germany, J. Singer and R. Staufenbiel, eds., Oct. 12-17, 1980, pp. 417-428.
17. Schewe, G.: On the Force Fluctuations Acting on a Circular Cylinder in Crossflow from Subcritical up to Transcritical Reynolds Numbers. J. Fluid Mech., vol. 133, 1983, pp. 265-285.
18. Joseph, D. D.: Hydrodynamic Stability and Bifurcation in Hydrodynamic Instabilities and the Transition to Turbulence. Topics in Applied Physics, vol. 45, H. L. Swinney and J. P. Gollub, eds., Springer-Verlag, Berlin, 1981, pp. 27-76.
19. McAlister, K. W.: A Pulse-Forming Network for Particle Path Visualization. NASA TM-81311, 1981.

WATER TUNNEL MODEL INSTALLATION

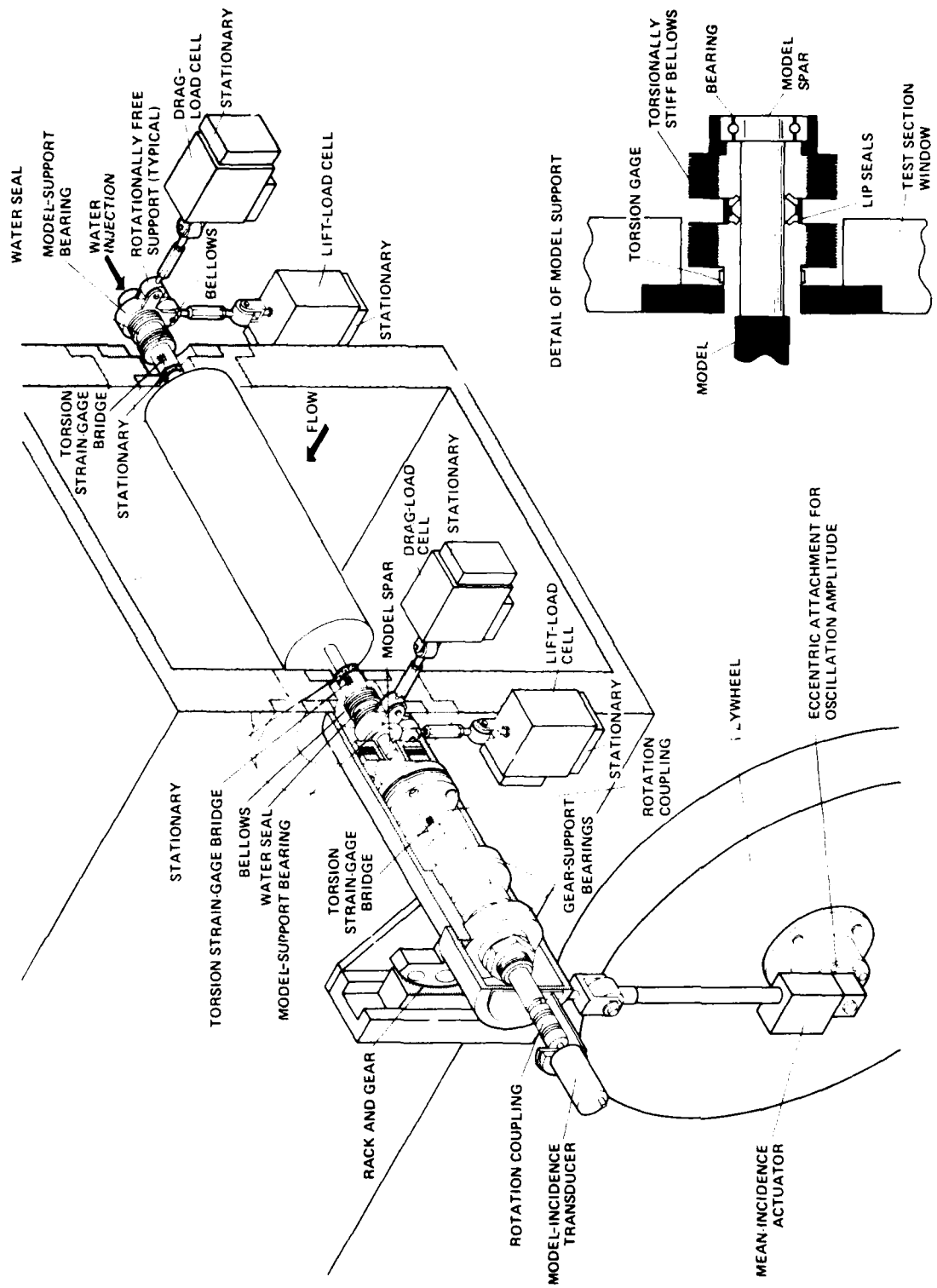


Figure 1.- Model installation and balance system for measuring lift and drag.

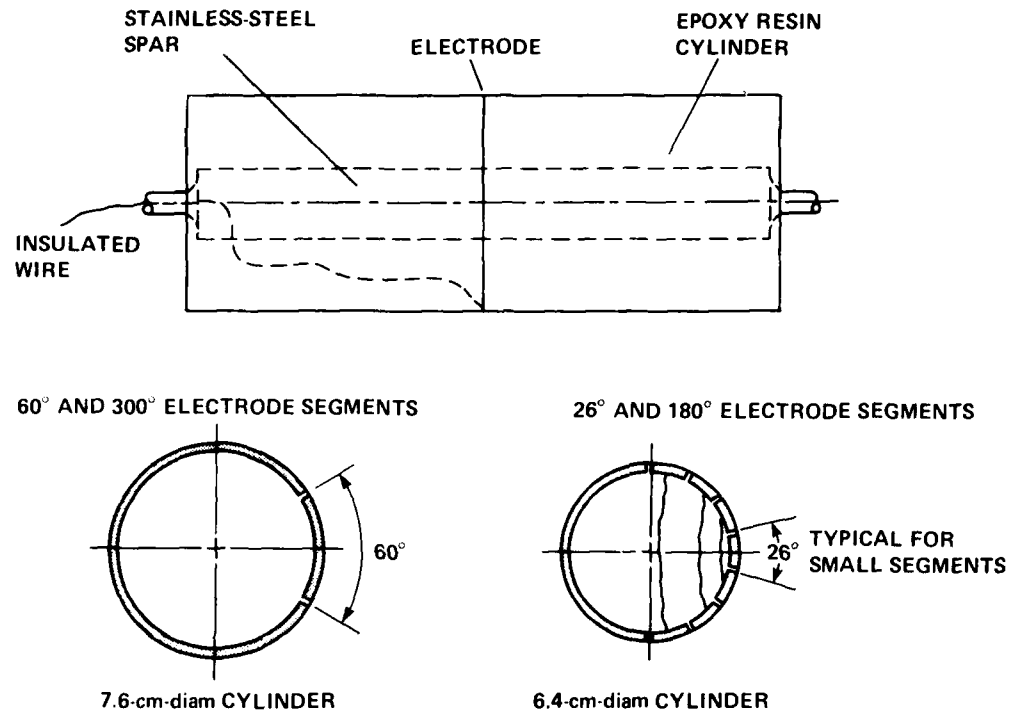


Figure 2.—Cylindrical models showing placement of electrodes.

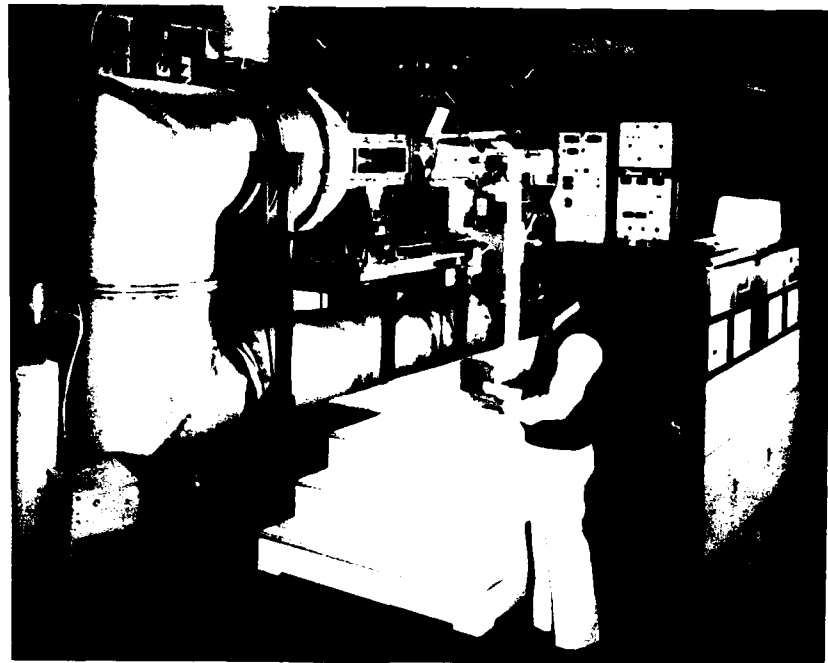


Figure 3.— Aeromechanics 21- by 31-cm Water Tunnel.

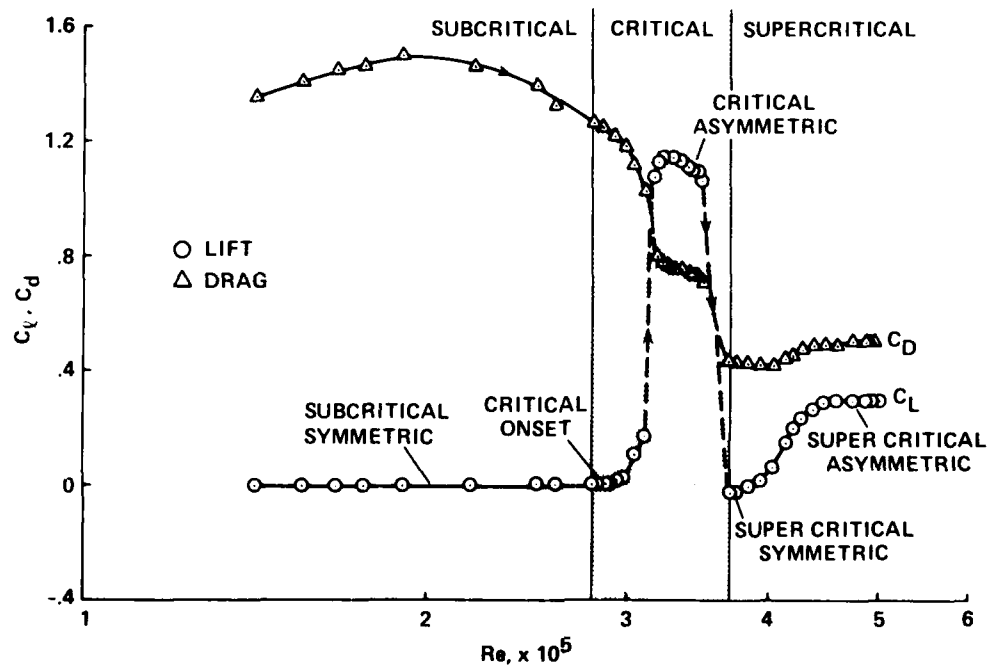
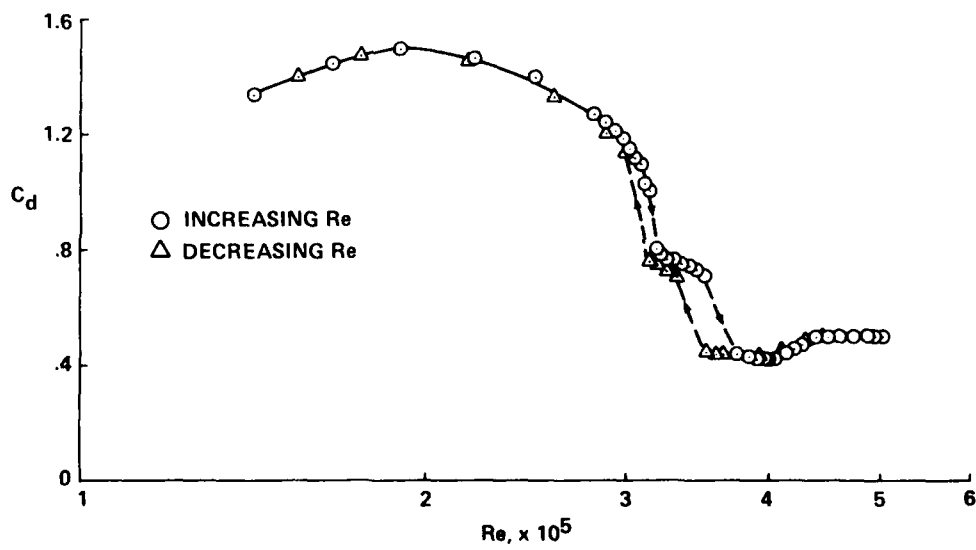
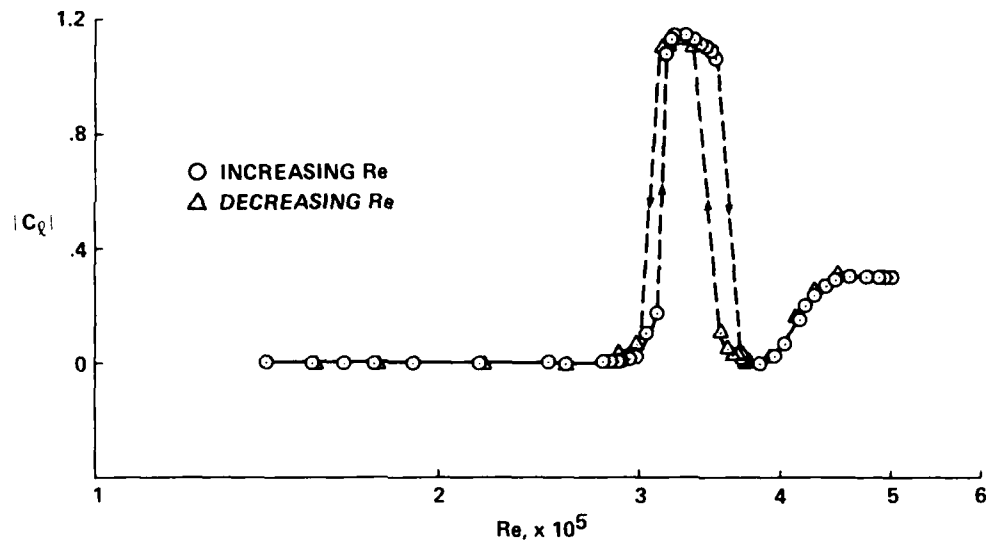


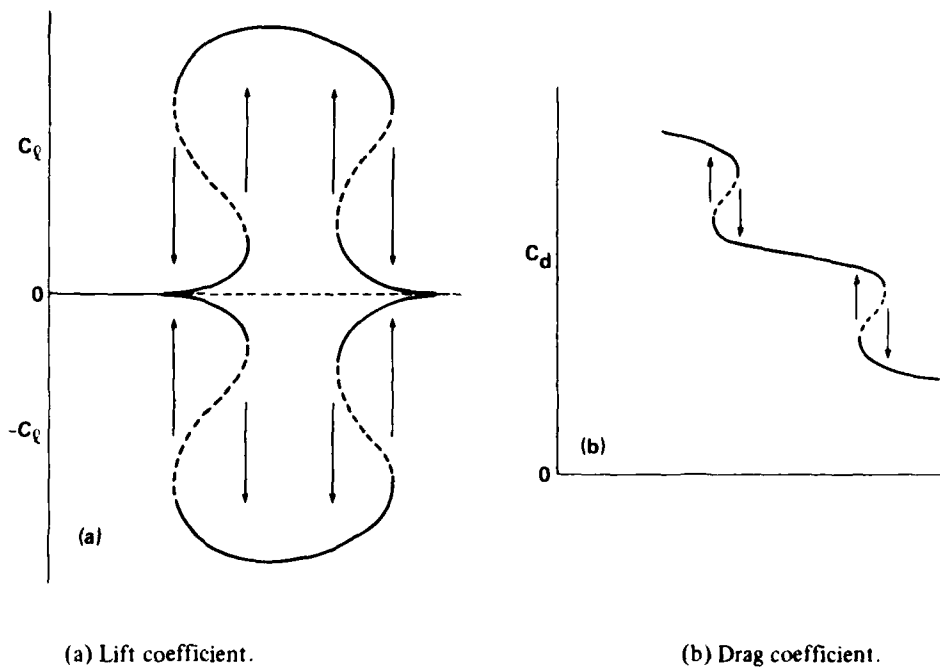
Figure 4.— Average lift and drag coefficients for the 6.4-cm-diam cylinder.



(a) Lift coefficient.

(b) Drag coefficient.

Figure 5. - Hysteresis in the load curves for the 6.4-cm-diam cylinder.



(a) Lift coefficient.

(b) Drag coefficient.

Figure 6.— Exaggerated supercritical bifurcations based on measured loads.

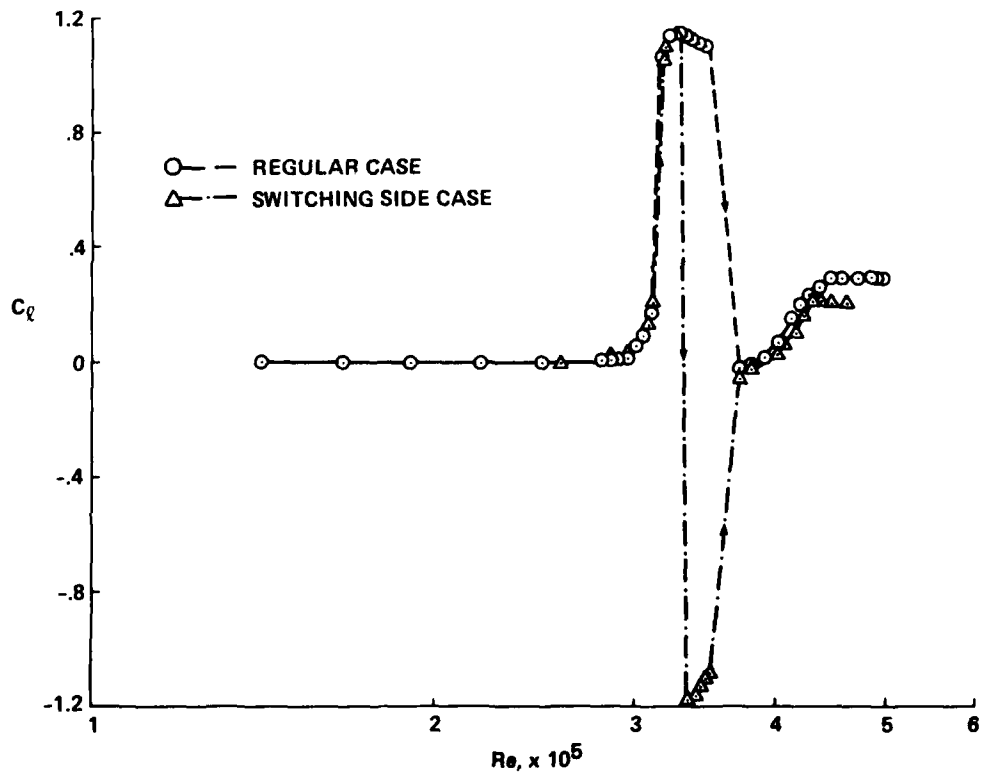
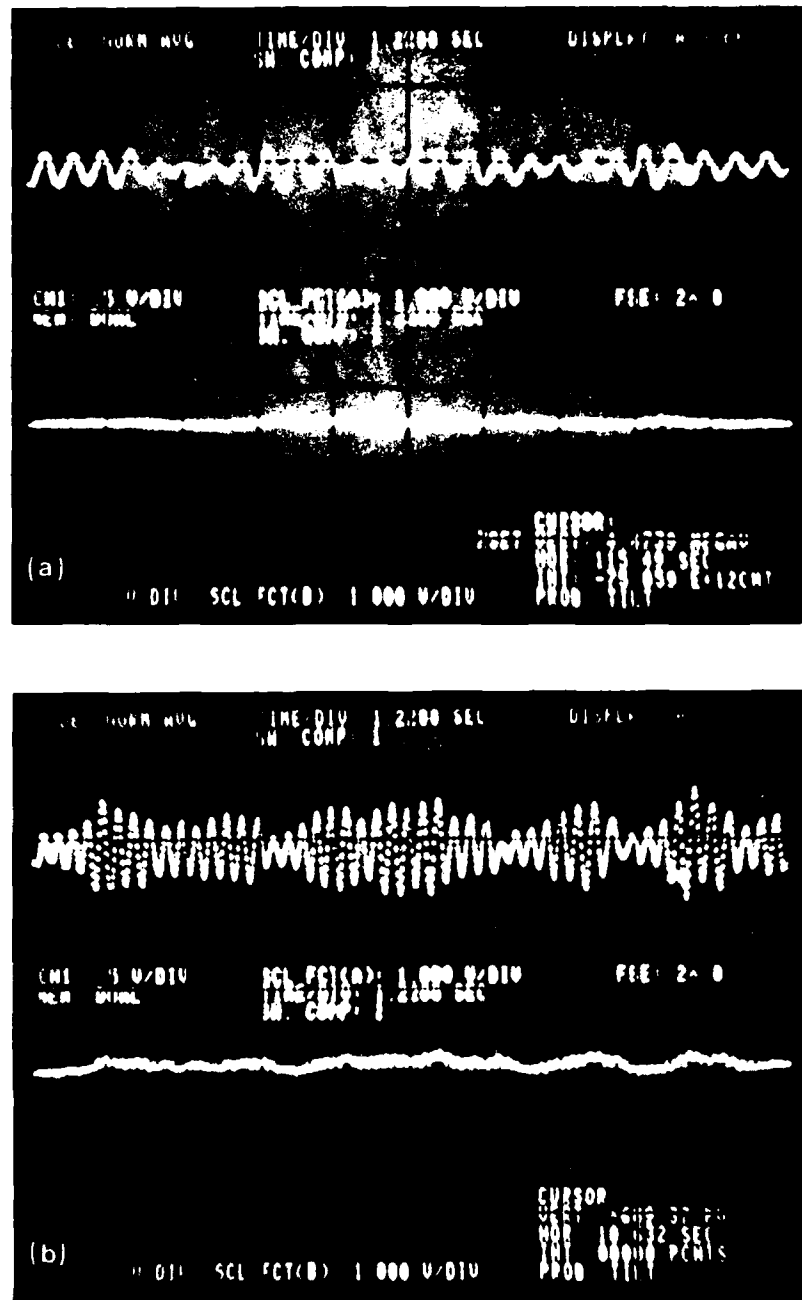
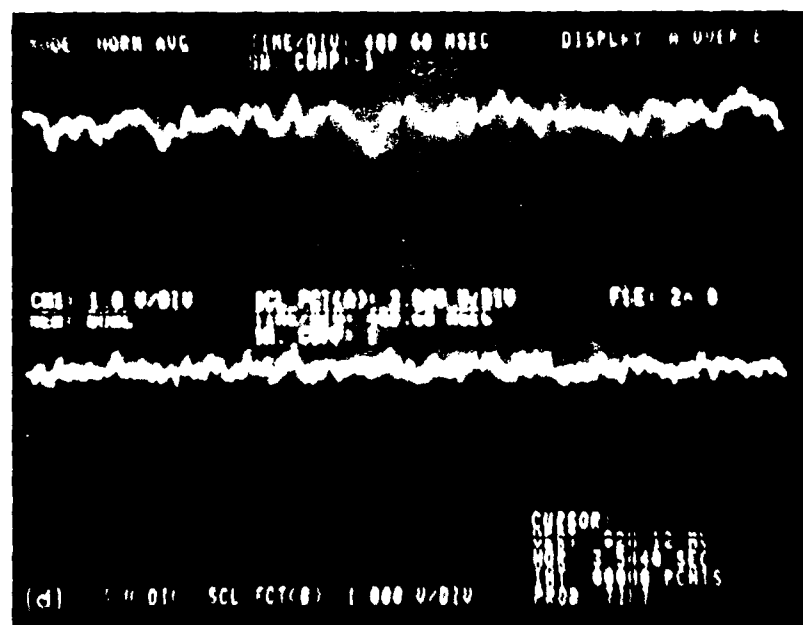
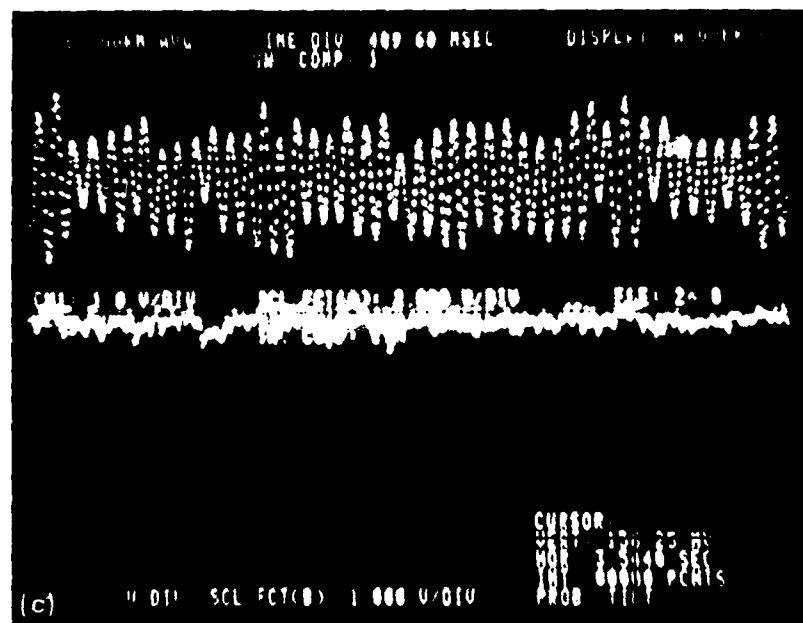


Figure 7.— An example of the asymmetric flow changing sides on the 6.4-cm-diam cylinder.



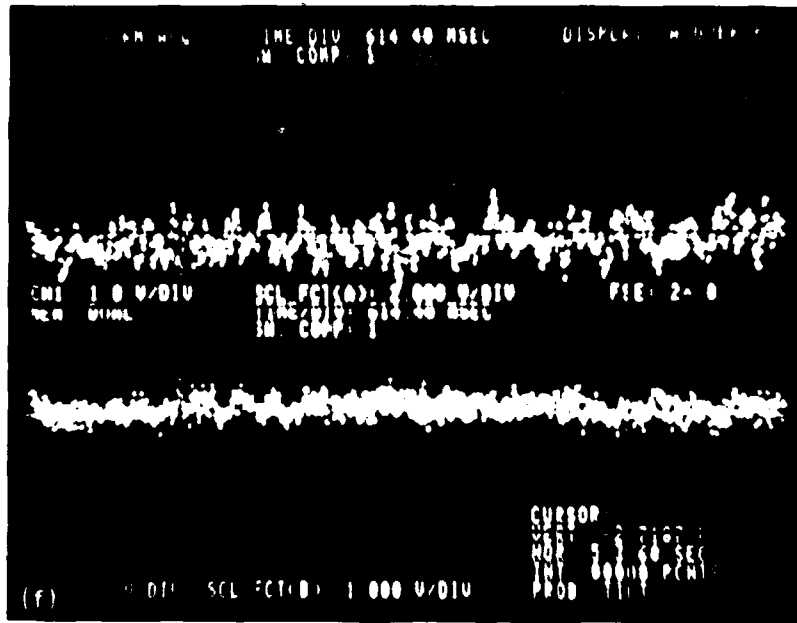
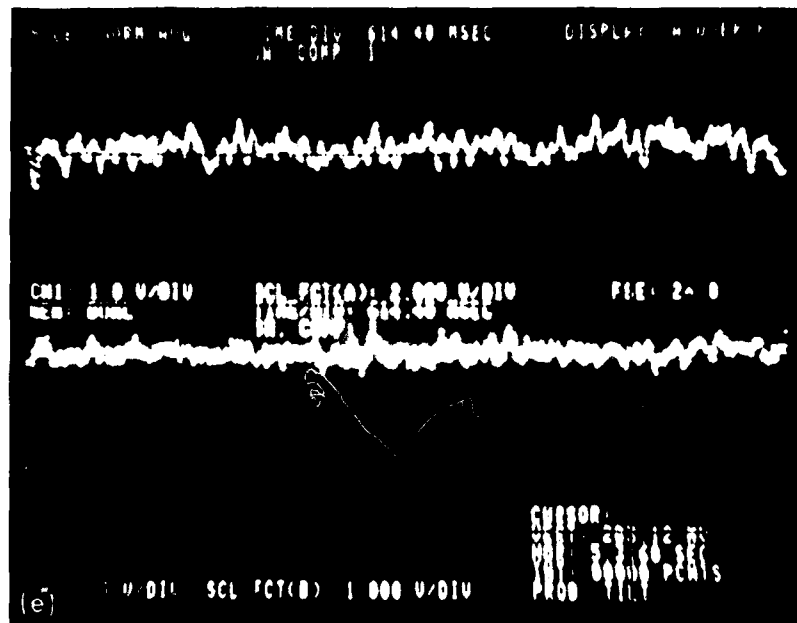
(a)  $Re = 50,000$ ; subcritical.  
 (b)  $Re = 100,000$ ; subcritical with pronounced beat.

Figure 8.— Analog traces of the lift and drag loads at various Reynolds numbers on the 7.6-cm-diam cylinder.



(c)  $Re = 225,000$ ; subcritical.  
 (d)  $Re = 250,000$ ; critical onset.

Figure 8.—Continued.



(e)  $Re = 262,500$ ; critical asymmetric.  
(f)  $Re = 375,000$ ; supercritical symmetric.

Figure 8.— Concluded.

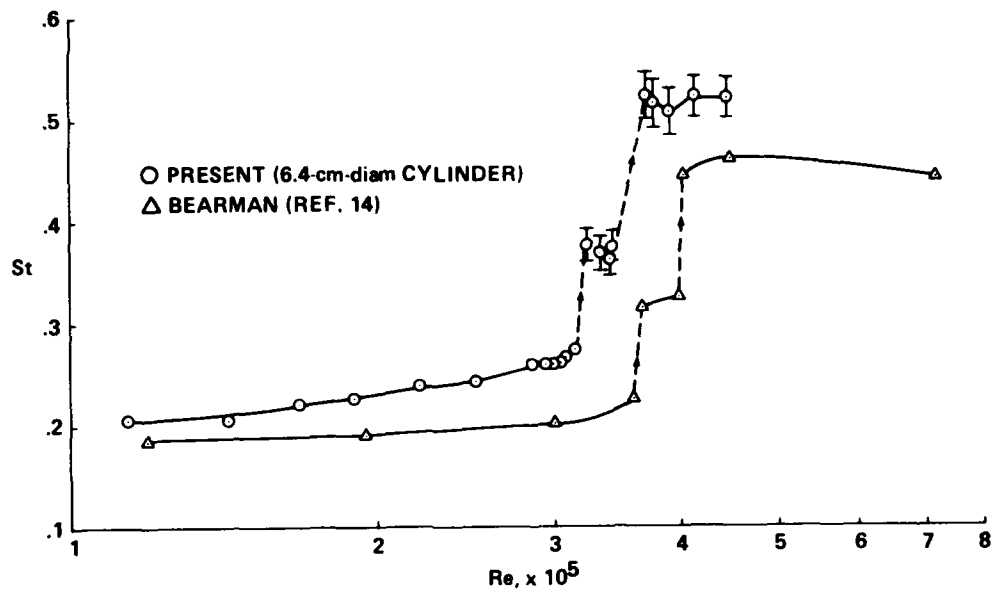


Figure 9.— Variation of the Strouhal number with Reynolds number on the 6.4-cm-diam cylinder.

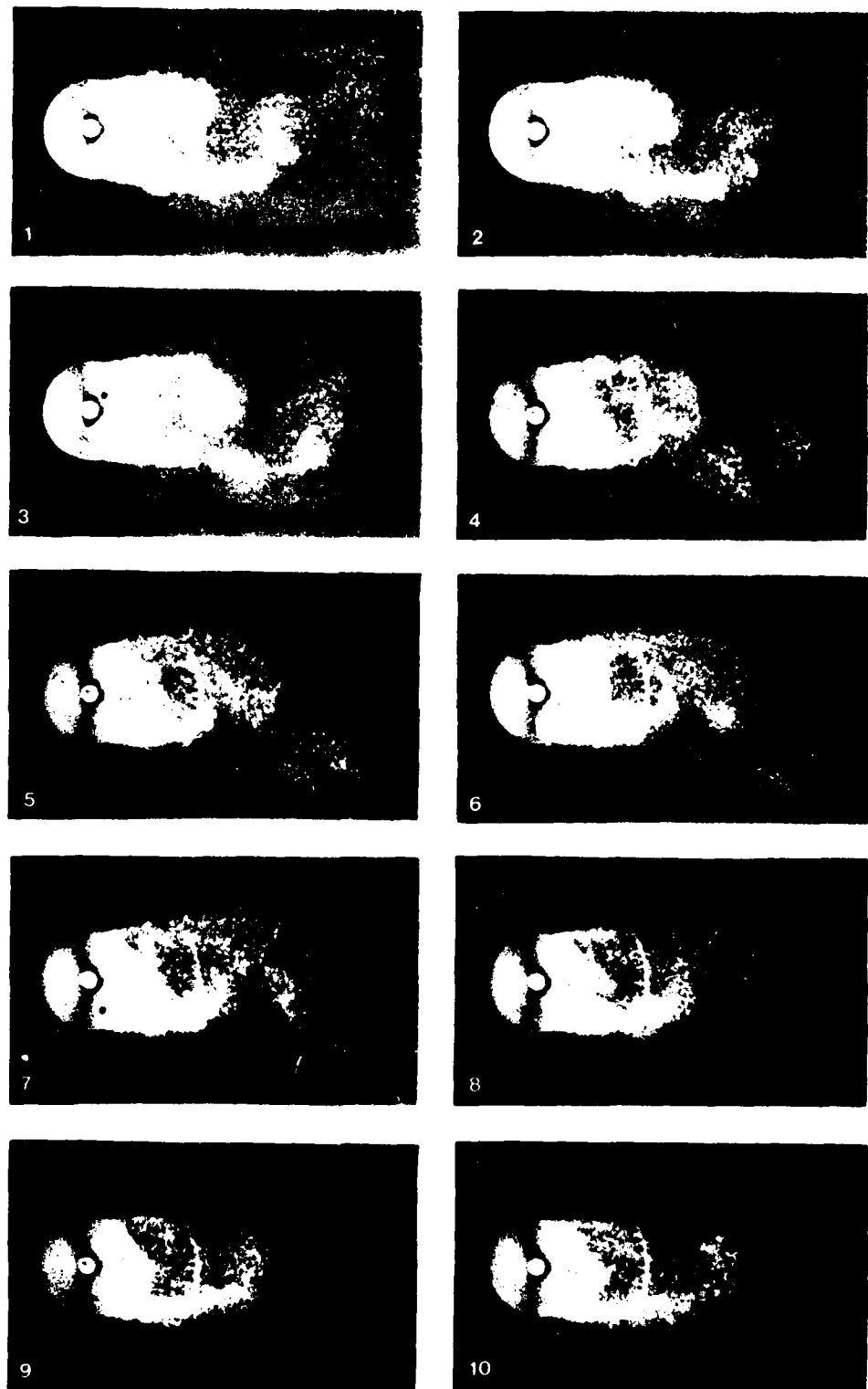
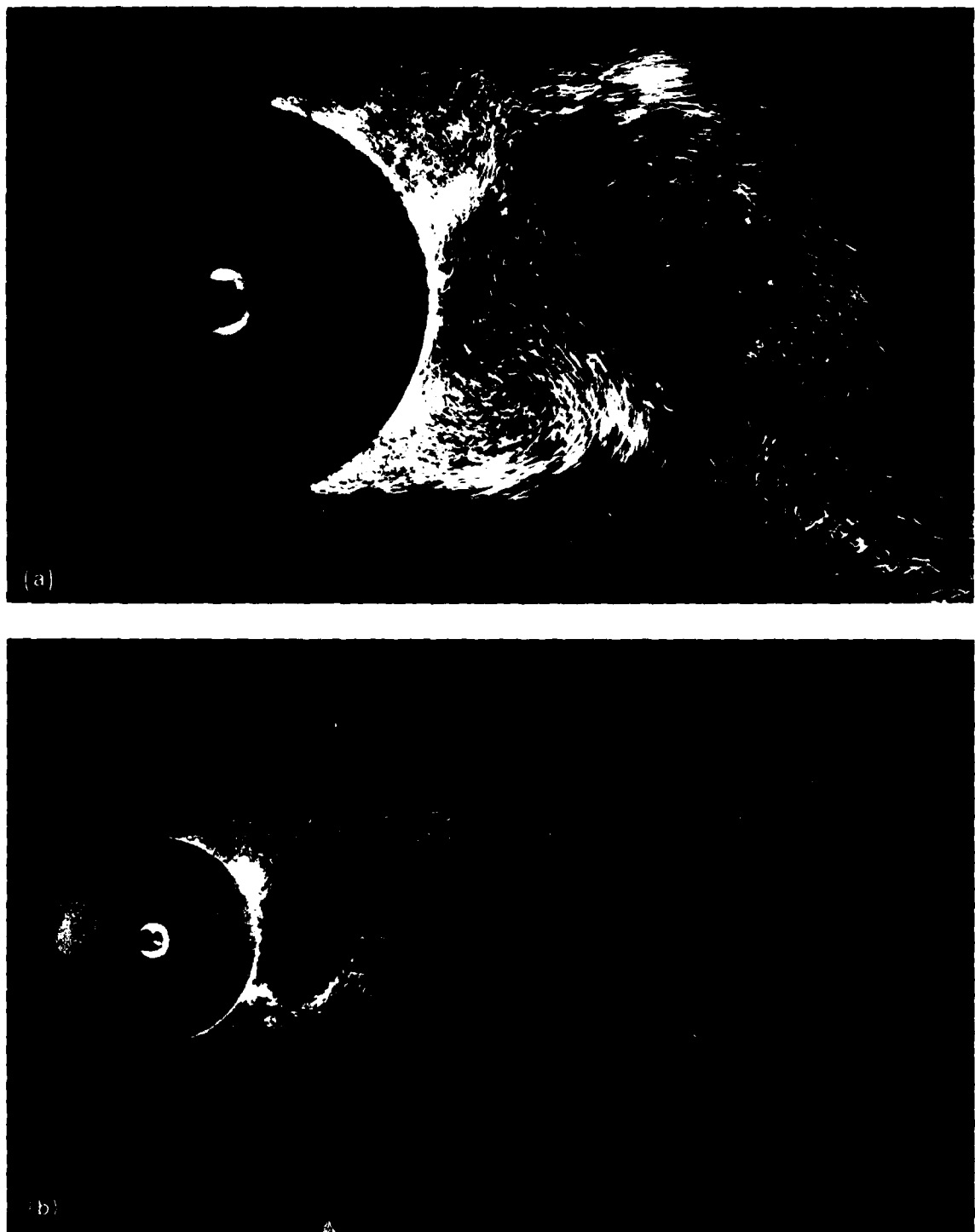


Figure 10. Movie sequence for the 6.4-cm-diam cylinder at  $Re = 144,000$  (subcritical flow).



(a) Normal lens.  
(b) Wide-angle lens.

Figure 11. Path-line exposures taken at different times for the 6.4-cm-diam cylinder at  $Re = 144,000$  (subcritical flow).

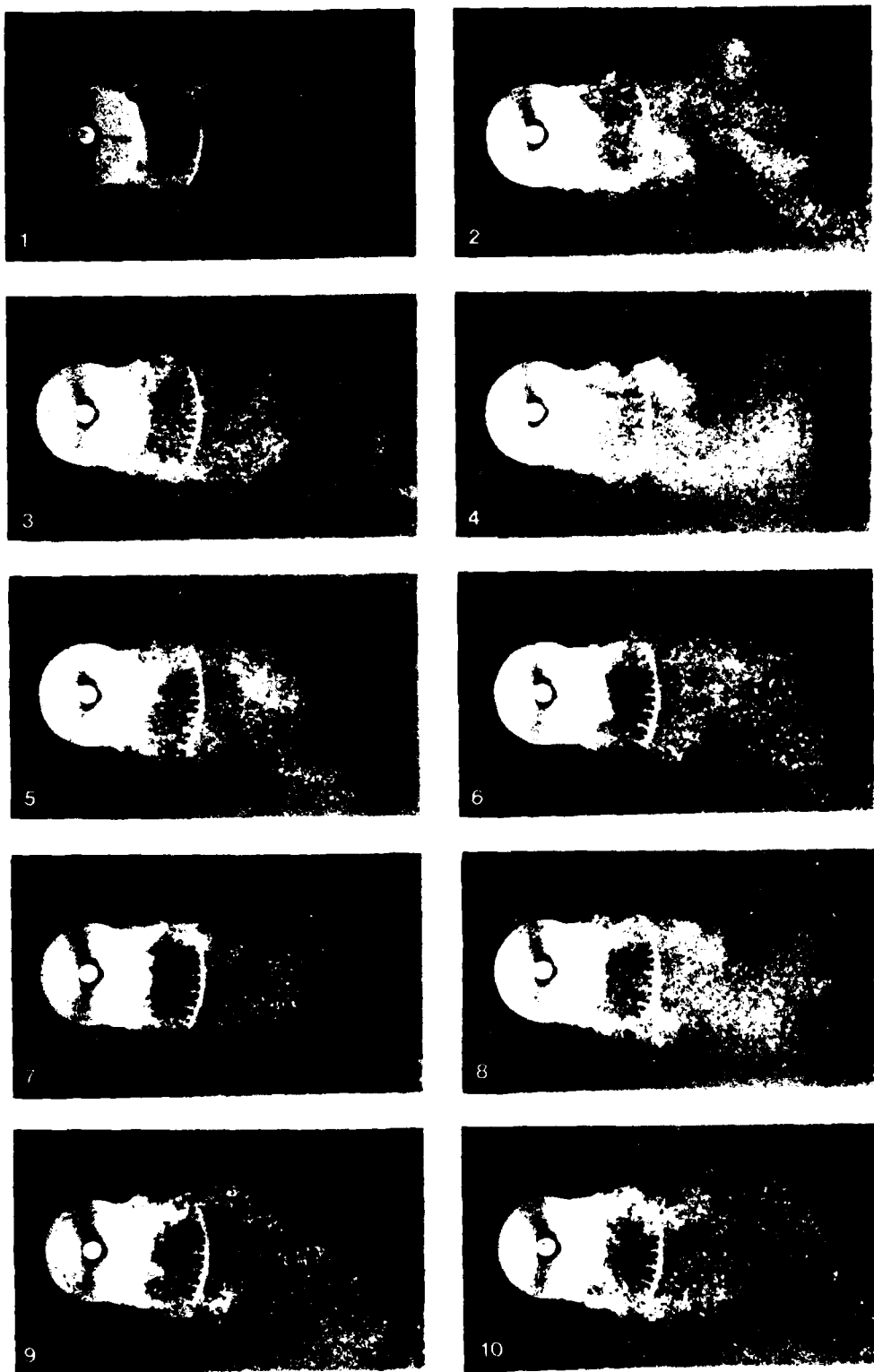
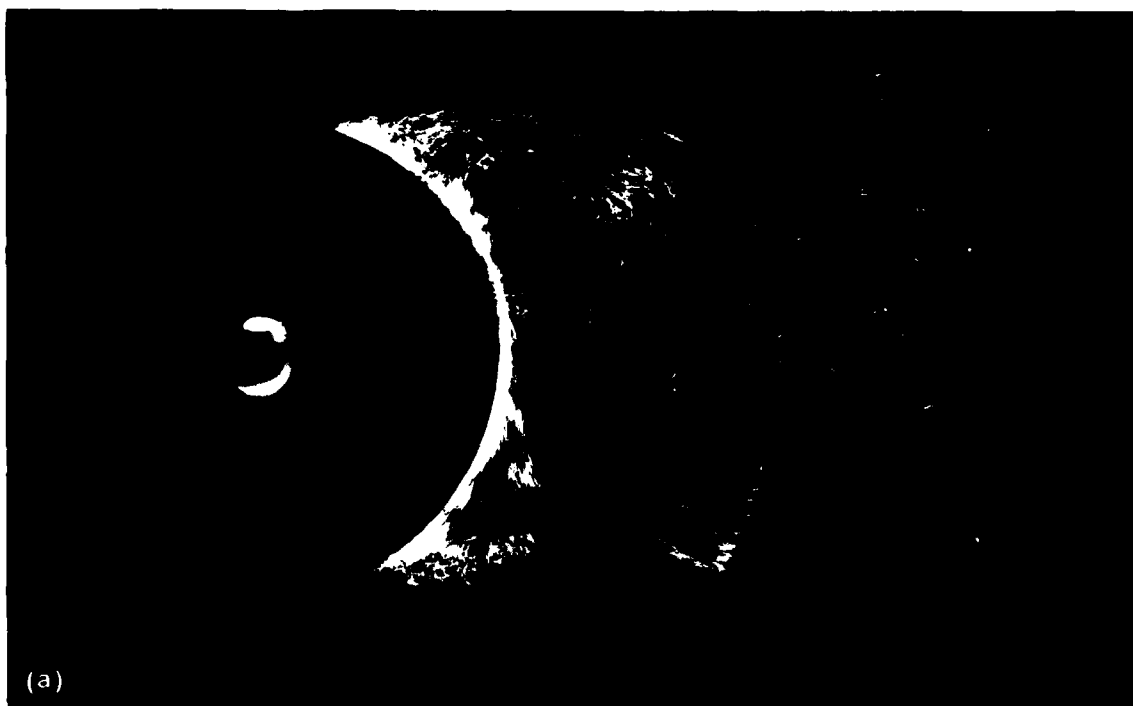


Figure 12. – Movie sequence for the 6.4-cm-diam cylinder at  $Re = 308,000$  (critical onset flow).



(a)



(b)

(a) Normal lens.  
(b) Wide-angle lens.

Figure 13. Path-line exposures for the 6.4-cm-diam cylinder at  $Re = 308,000$  (critical onset flow).

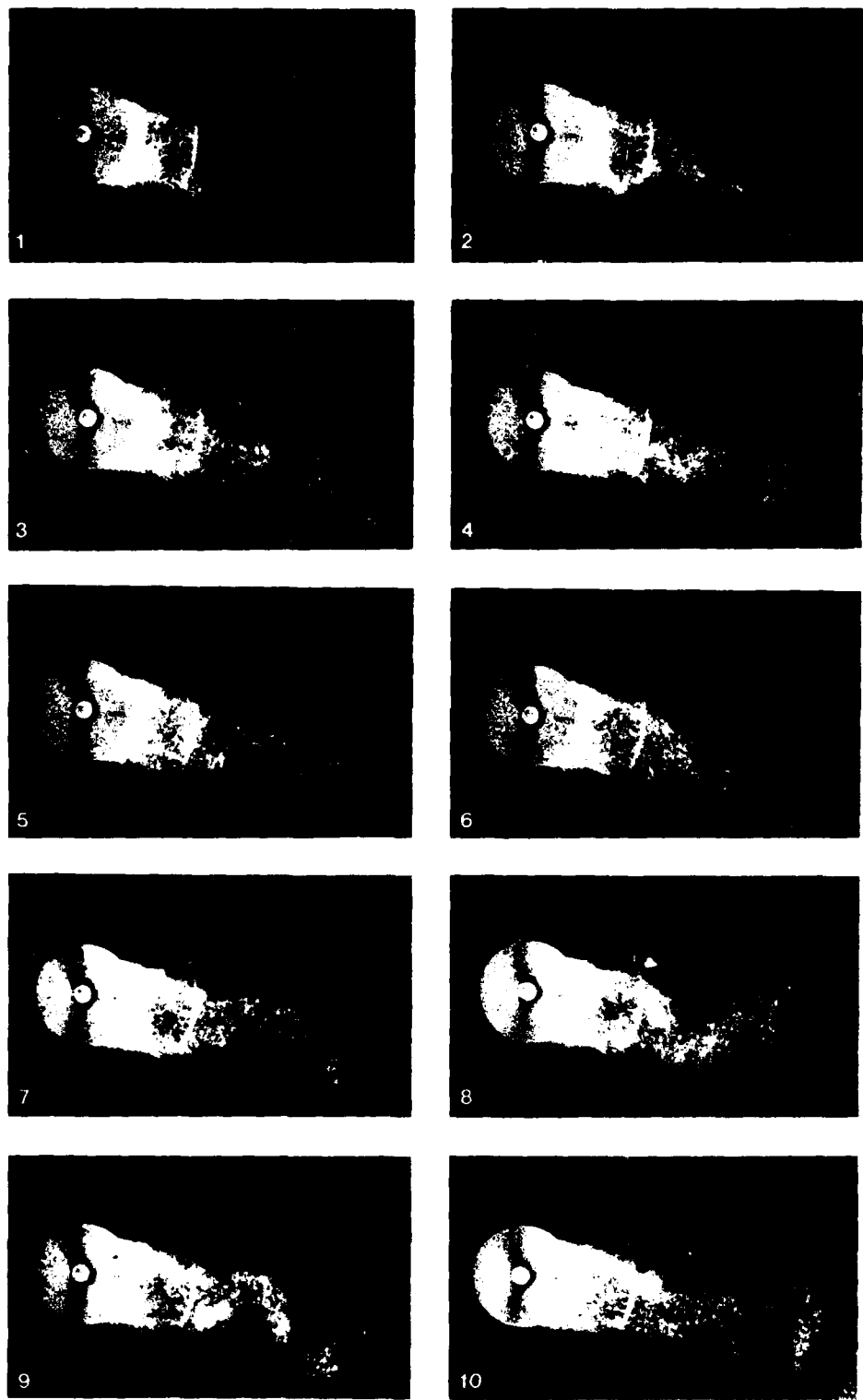


Figure 14.— Movie sequence for the 6.4-cm-diam cylinder at  $Re = 342,000$  (critical asymmetric flow).



(a)

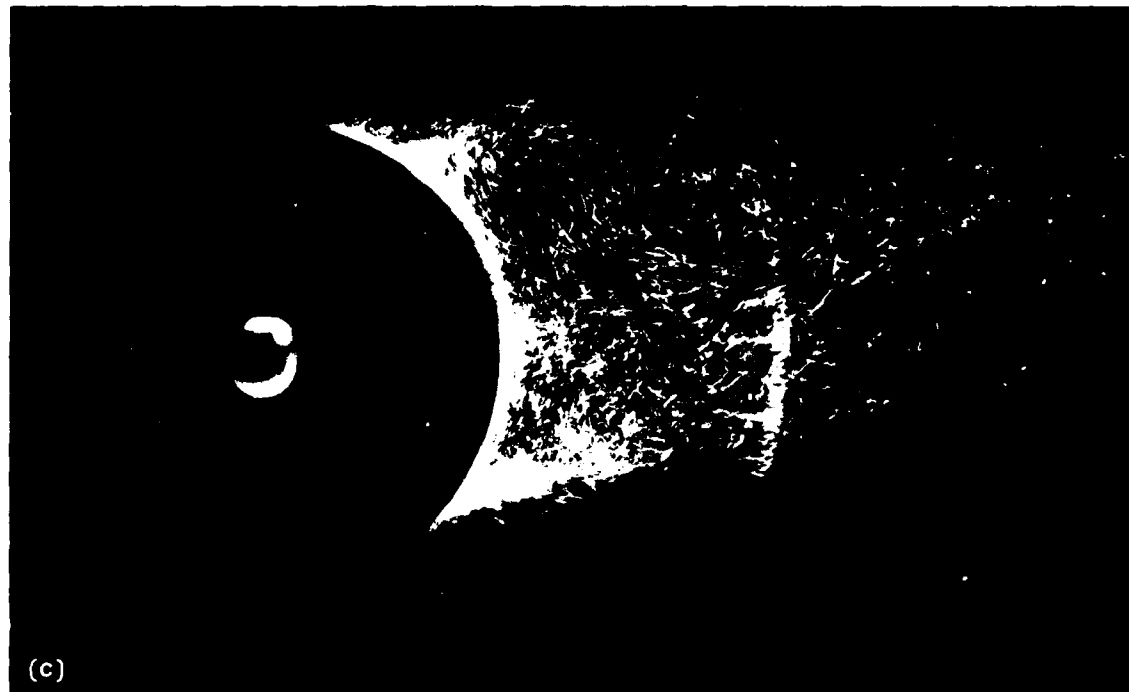


(b)

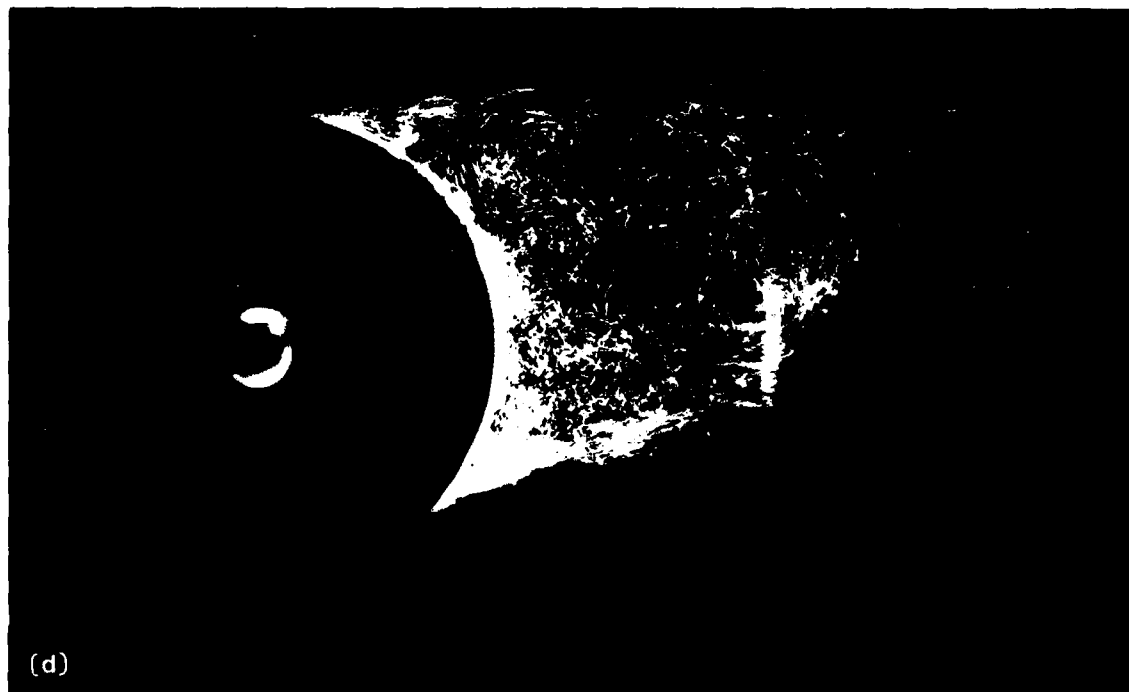
(a) Wide-angle lens,  $Re = 342,000$ .

(b) Asymmetry switched,  $Re = 347,000$ .

Figure 15. Path-line exposures for the 6.4-cm-diam cylinder in the critical asymmetric range.



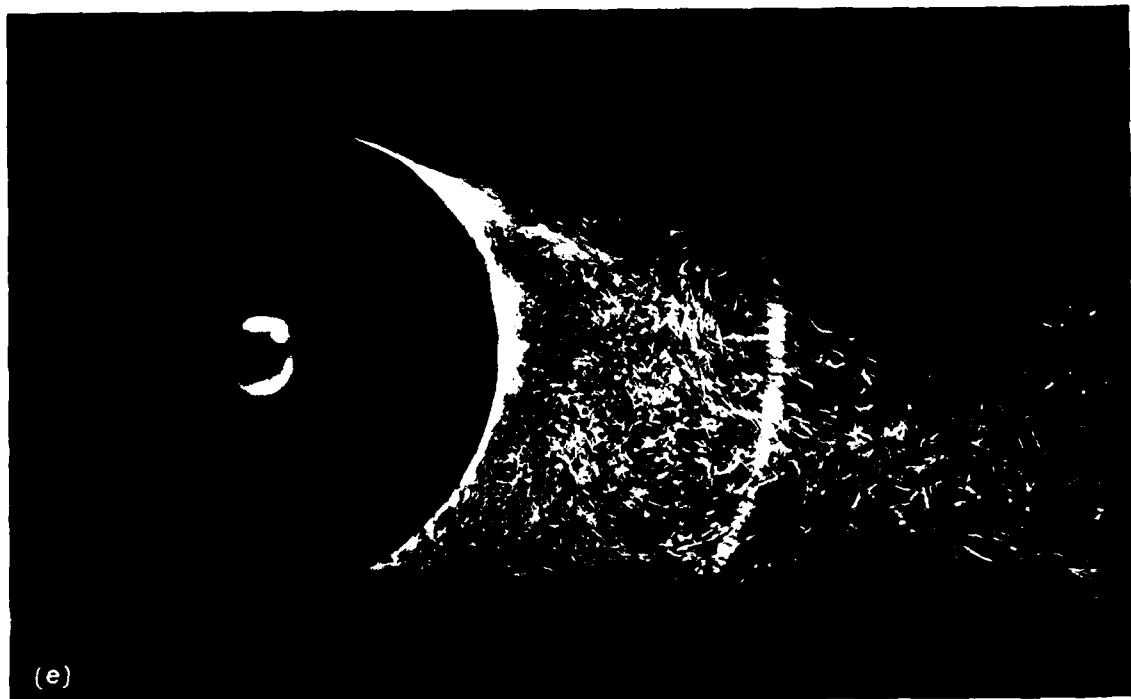
(c)



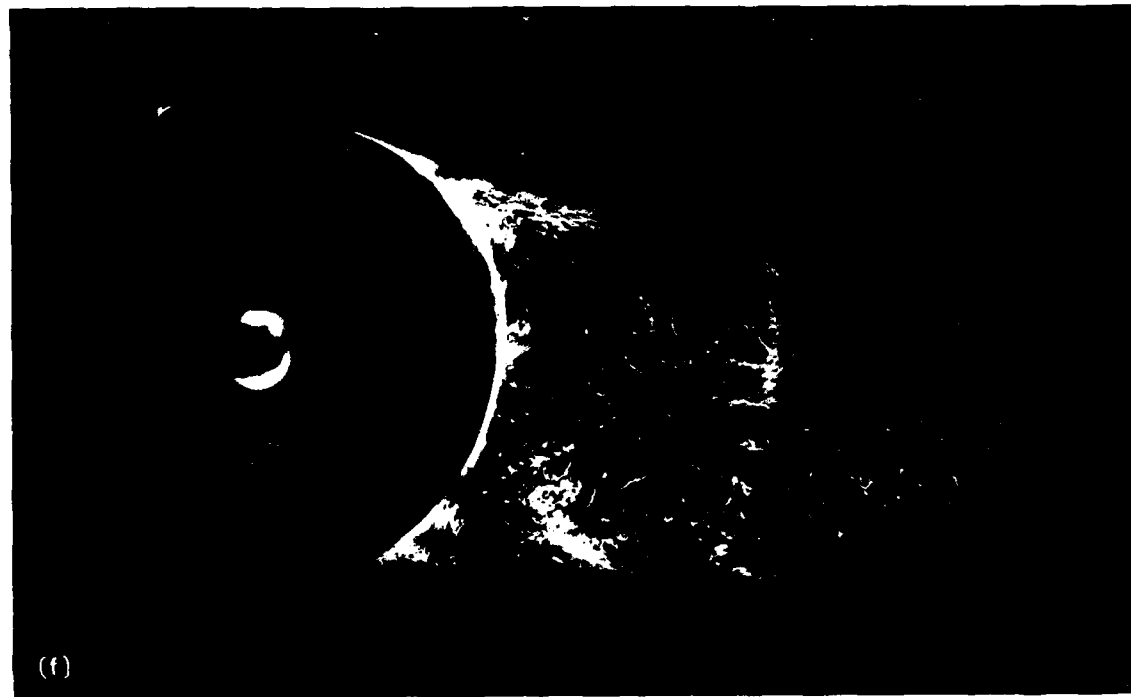
(d)

(c) Normal lens,  $Re = 338,000$ .  
(d) Same as above, except at different time.

Figure 15. Continued.



(e)



(f)

(e) Asymmetry switched,  $Re = 338,000$ .  
(f) Same as above, except  $Re = 342,000$ .

Figure 15. - Concluded.

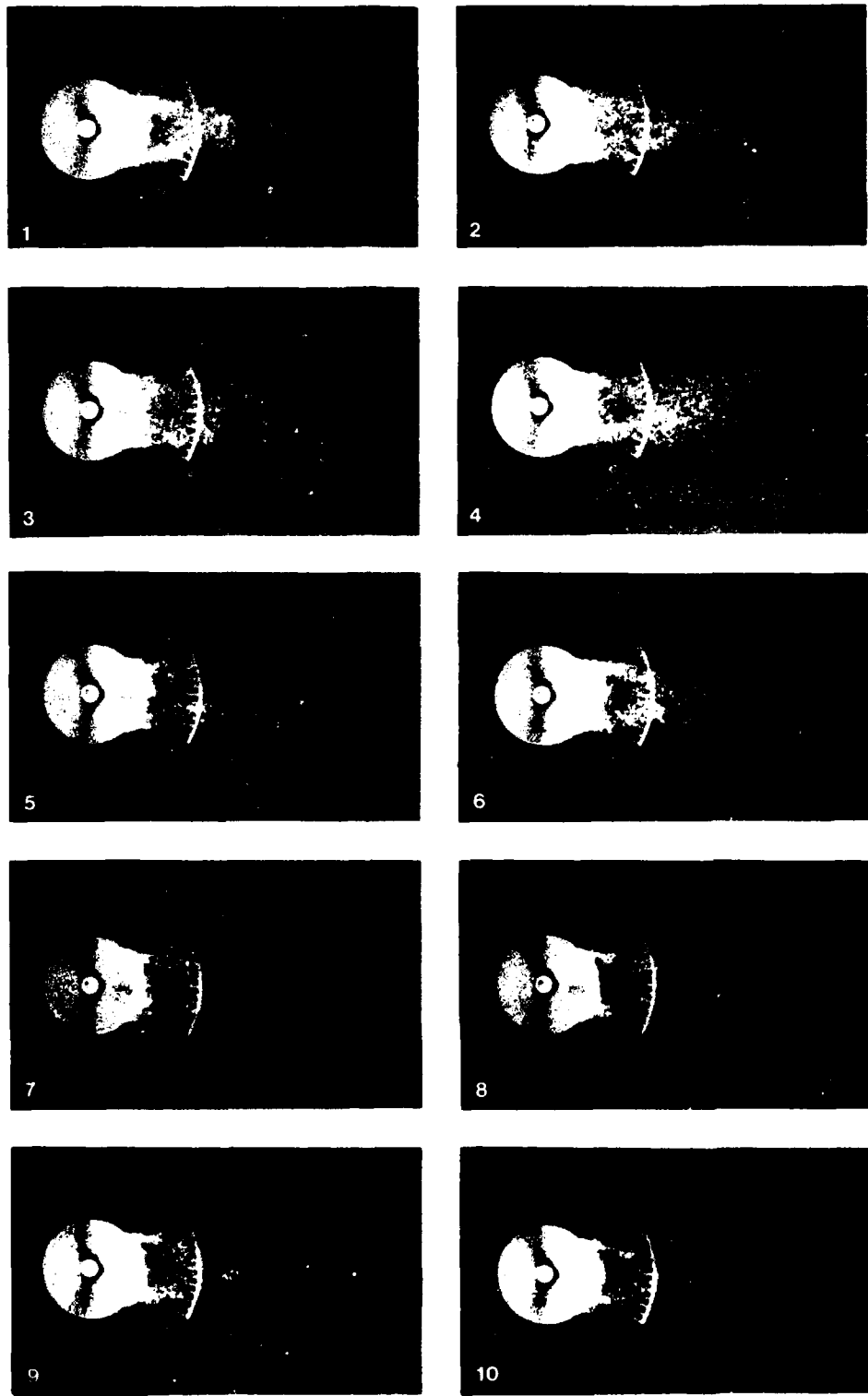
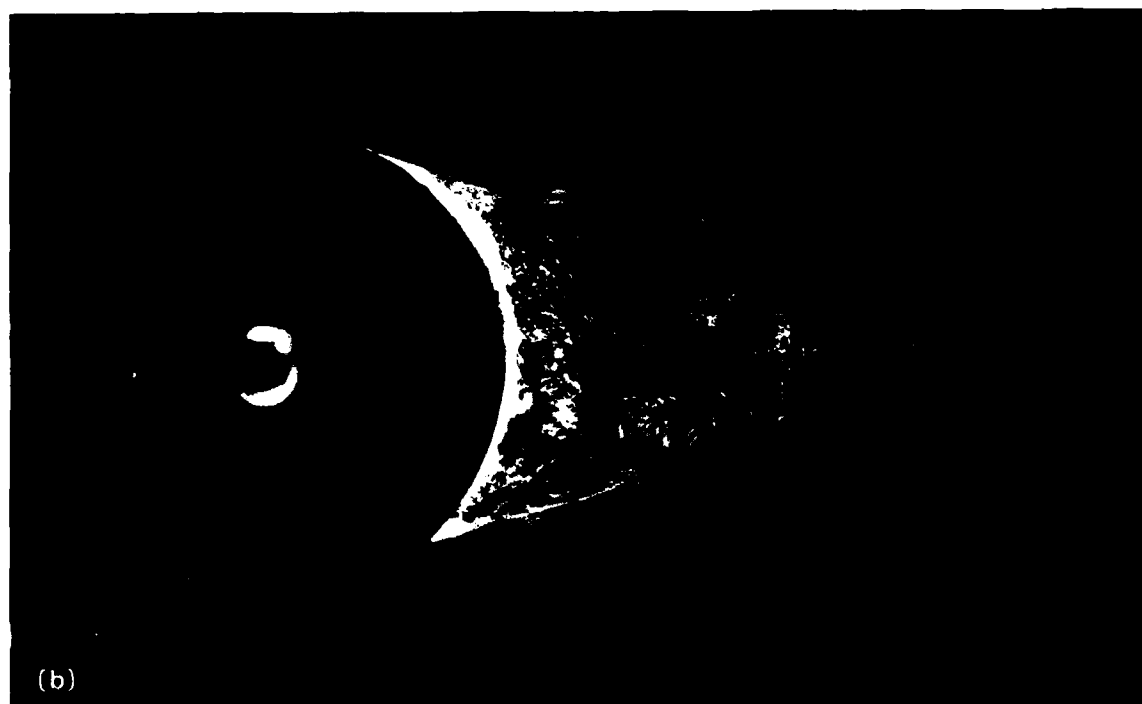


Figure 16. Movie sequence for the 6.4-cm-diam cylinder at  $Re = 390,000$  (supercritical symmetric).



(a)



(b)

(a) Normal lens.  
(b) Same as above, except at different time.

Figure 17. Path-line exposures for the 6.4-cm-diam cylinder at  $Re = 374,000$  (supercritical symmetric).

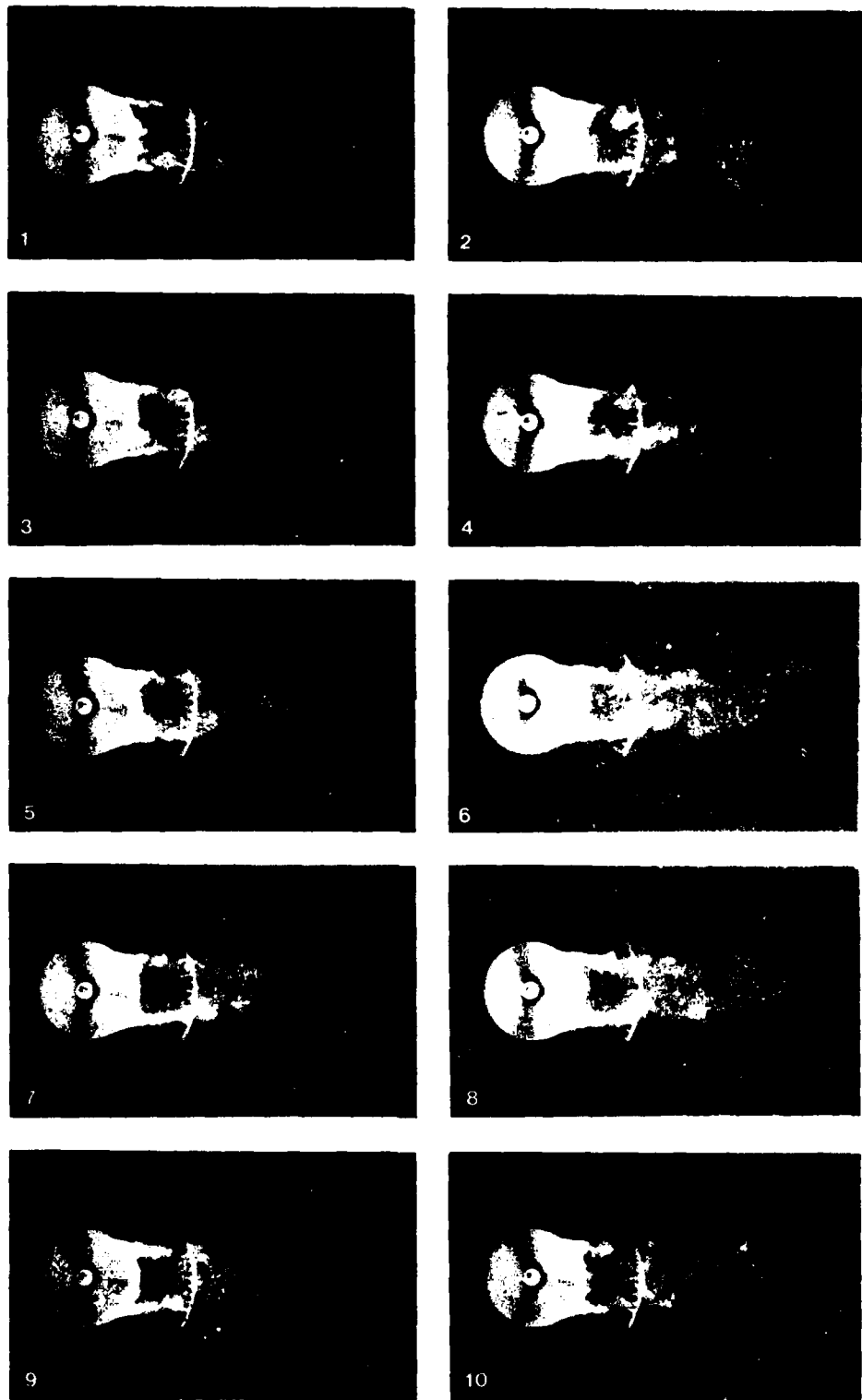
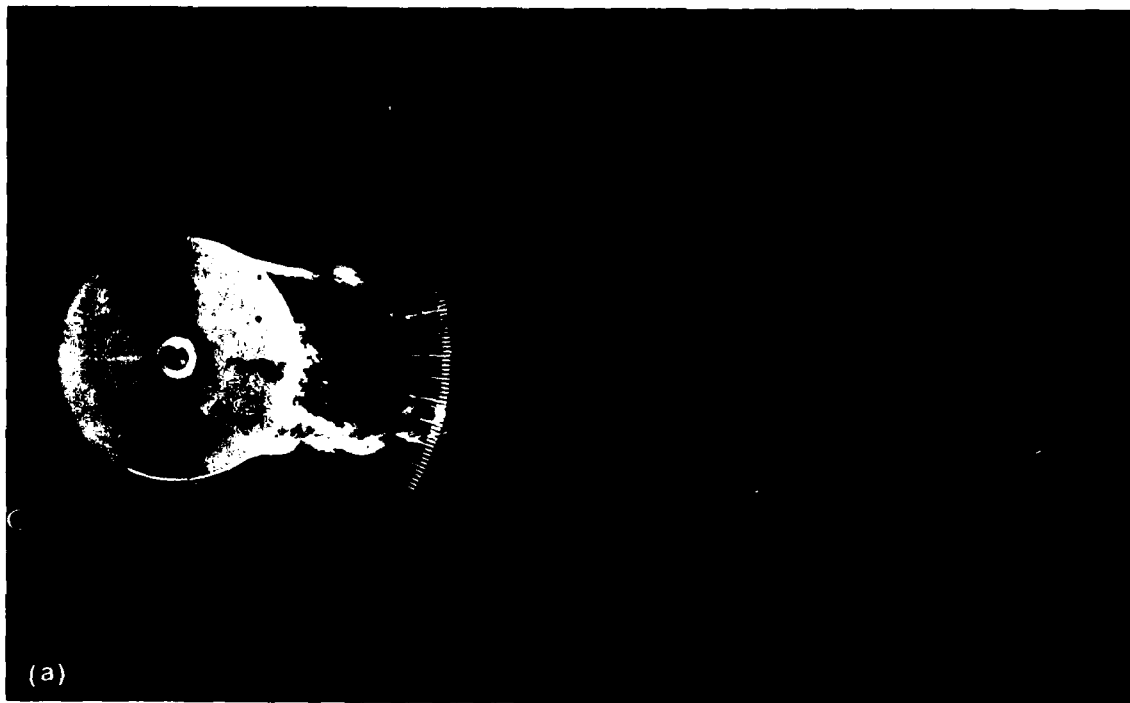


Figure 18.—Movie sequence for the 6.4-cm-diam cylinder at  $Re = 540,000$  (supercritical asymmetric).



(a)

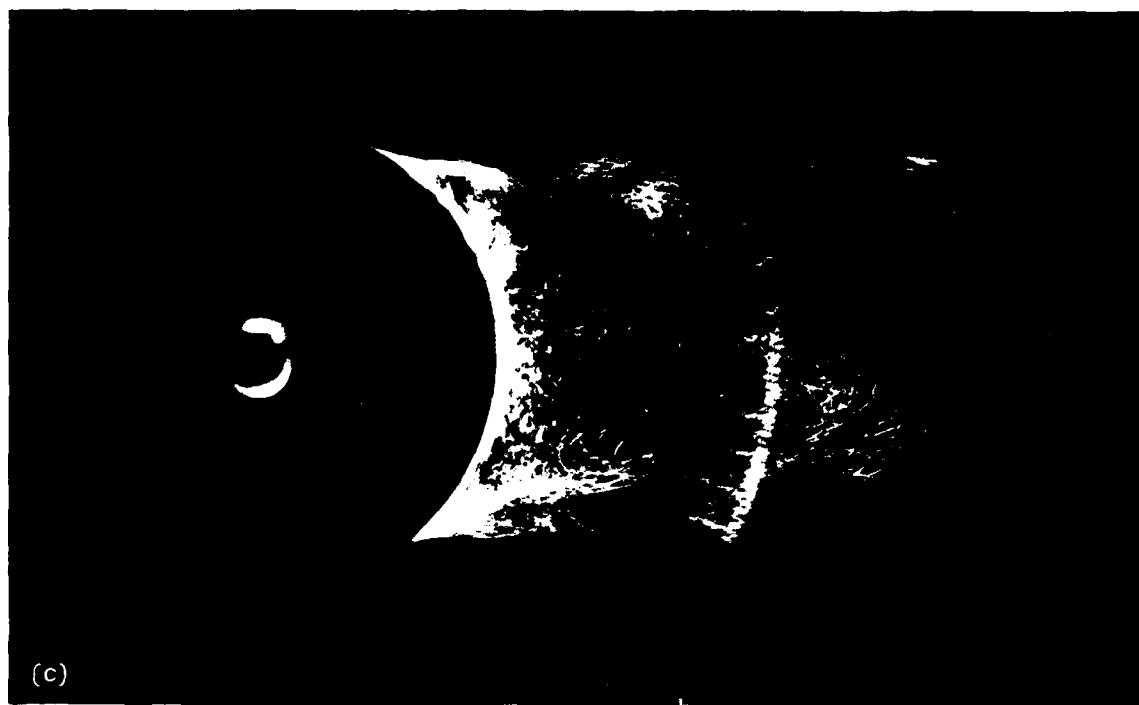


(b)

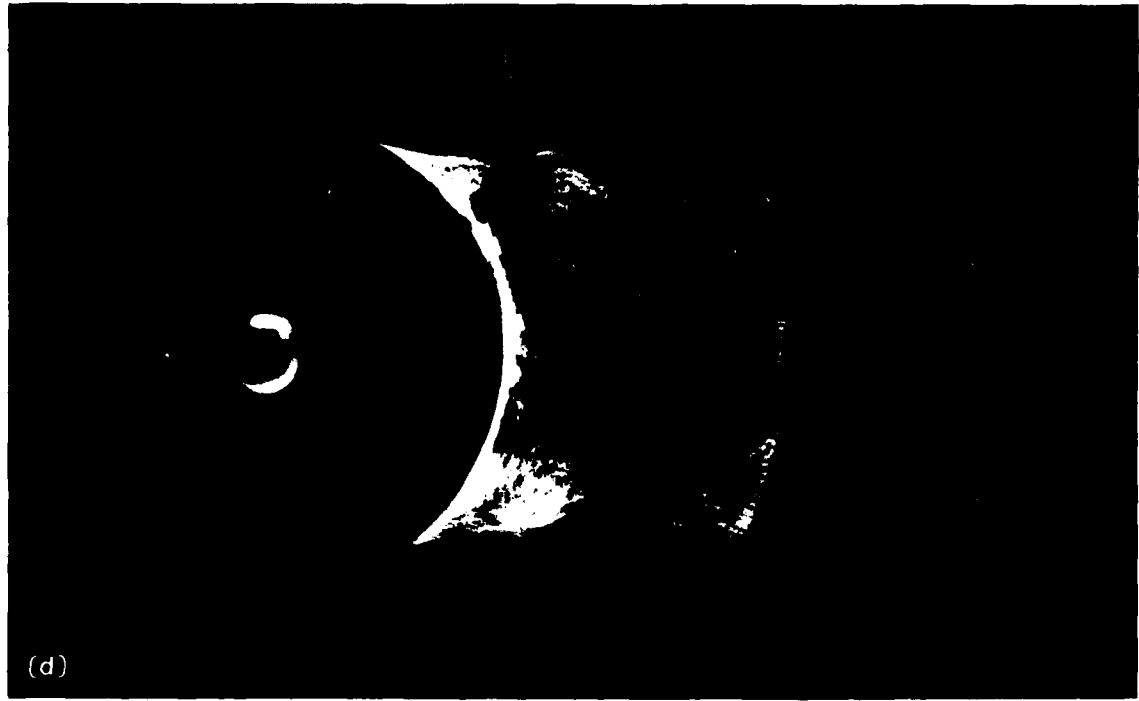
(a) Wide-angle lens.

(b) Same as above, except at different time.

Figure 19. Path-line exposures for the 6.4-cm-diam cylinder at  $Re = 540,000$  (supercritical asymmetric).



(c)



(d)

(c) Normal lens.  
(d) Same as above except at different time.

Figure 19. Concluded.

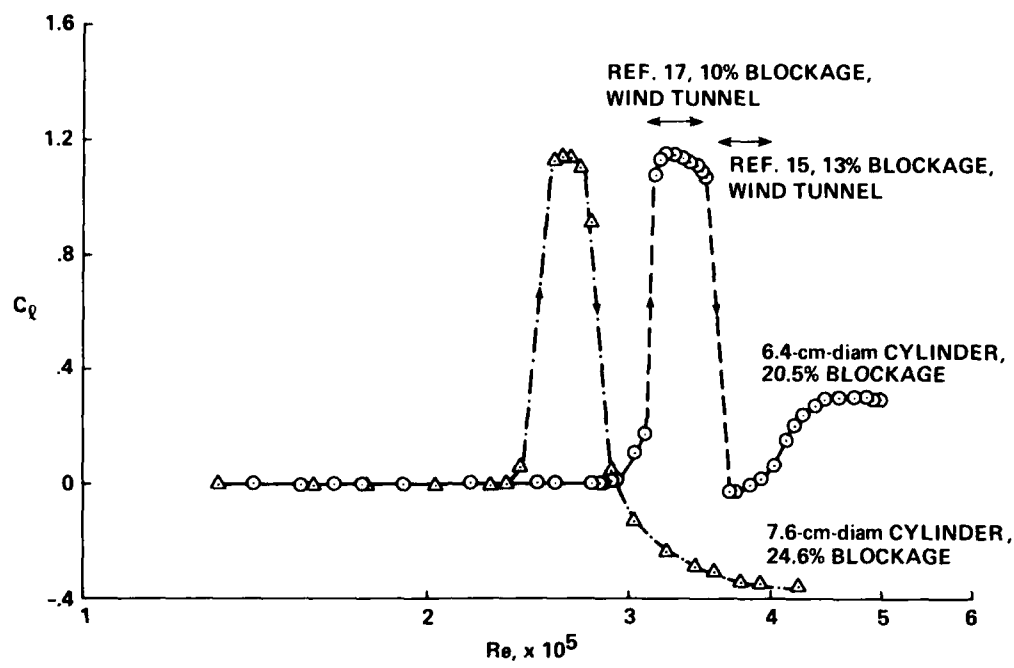


Figure 20.— Tunnel blockage effects on the asymmetric region.

1 Report No NASA TM-85879 AVSCOM TM 84-A-1	2. Government Accession No AD 3142267	3. Recipient's Catalog No.	
4. Title and Subtitle WATER-TUNNEL STUDY OF TRANSITION FLOW AROUND CIRCULAR CYLINDERS		5. Report Date May 1984	
7. Author(s) D. Almosnino* and K. W. McAlister		6. Performing Organization Code	
9. Performing Organization Name and Address Ames Research Center and Aeromechanics Laboratory, U.S. Army Research and Technology Laboratories - AVSCOM, Ames Research Center, Moffett Field, CA 94035		8. Performing Organization Report No. A-9606	
12 Sponsoring Agency Name and Address National Aeronautics and Space Administration, Washington, DC 20546 and U.S. Army Aviation Systems Command, St. Louis, MO 63120		10. Work Unit No. K-1585	
15 Supplementary Notes *NASA/NRC Research Associate from Israel. Point of Contact: Ken McAlister, Aeromechanics Laboratory, USAAVSCOM Research and Technology Laboratories, Ames Research Center, MS 215-1, Moffett Field, CA 94035 (415)965-5892 or FTS 448-5892.		11. Contract or Grant No.	
16 Abstract <i>C sub crit approx = to 1.2</i>		13. Type of Report and Period Covered Technical Memorandum	
<p>The recently reported phenomenon of asymmetric flow separation from a circular cylinder in the critical Reynolds number regime has been confirmed in a water-tunnel experiment. For the first time, an attempt was made to visualize the wake of the cylinder during the transition from subcritical to critical flow and to correlate the visualizations with lift and drag measurements. The occurrence of a dominant asymmetric-flow state was quite repeatable, both when increasing and decreasing the Reynolds number, resulting in a mean lift coefficient of <math>C_L \approx 1.2</math> and a shift in the angle of the wake by about <math>12^\circ</math>. A distinctive step change in the drag and shedding frequency was also found to occur. A hysteresis was confirmed to exist in this region as the Reynolds number was cycled over the transition range. Both boundaries of the asymmetry appear to be supercritical bifurcations in the flow. The asymmetry was normally steady in the mean; however, there were instances when the direction of the asymmetry reversed and remained so for the duration of the Reynolds number sweep through this transition region. A second asymmetry was observed at a higher Reynolds number; however, the mean lift coefficient was much lower, and the direction of the asymmetry was not observed to reverse. Introducing a small local disturbance into the boundary layer was found to prevent the critical asymmetry from developing along the entire span of the cylinder.</p>		14. Sponsoring Agency Code 505-31-21	
17. Key Words (Suggested by Author(s)) Cylinder Wake flow Asymmetric flow Flow bifurcation		18. Distribution Statement Unclassified - Unlimited	
		Subject Category 02	
19. Security Classif. (of this report) Unclassified	20. Security Classif. (of this page) Unclassified	21. No. of Pages 34	22. Price* A03

\*For sale by the National Technical Information Service, Springfield, Virginia 22161

NASA-Langley, 1984

## WAKE FROM A CIRCULAR CYLINDER



Almosino & McAlister  
Ames Research Center  
Moffett Field, California